ChemPubSoc Europe

DOI: 10.1002/chem.201504932

CHEMISTRY A European Journal Full Paper

Molecular Recognition

Interactions of Enolizable Barbiturate Dyes

Alexander Schade,[a] Katja Schreiter,[a] Tobias Rüffer,[b] Heinrich Lang,[b] and Stefan Spange*[a]

Abstract: The specific barbituric acid dyes 1-*n*-butyl-5-(2,4-dinitro-phenyl) barbituric acid and 1-*n*-butyl-5-{4-[(1,3-dioxo-1*H*-inden-(3*H*)-ylidene)methyl]phenyl}barbituric acid were used to study complex formation with nucleobase derivatives and related model compounds. The enol form of both compounds shows a strong bathochromic shift of the UV/Vis absorption band compared to the rarely coloured keto form. The keto–enol equilibria of the five studied dyes are strongly dependent on the properties of the environment as shown by solvatochromic studies in ionic liquids and a set of organic solvents. Enol form development of the barbituric acid dyes is also associated with alteration of the hydrogen bonding pattern from the ADA to the DDA type (A = hydrogen bond acceptor site, D = donor site). Receptor-induced altering of ADA towards DDA hydrogen bonding patterns of the chromophores are utilised to study supramolecular complex formation. As complementary receptors 9-ethyladenine, 1-*n*-butylcytosine, 1-*n*-butylthymine, 9-ethylguanidine and 2,6-diacetamidopiridine were used. The UV/Vis spectroscopic response of acid–base reaction compared to supramolecular complex formation is evaluated by ^{1}H NMR titration experiments and X-ray crystal structure analyses. An increased acidity of the barbituric acid derivative promotes genuine salt formation. In contrast, supramolecular complex formation is preferred for the weaker acidic barbituric acid.

Introduction

The pairing of nucleobases and of related model compounds by multiple hydrogen bonds is a fascinating field of research owing to its importance in nature.[1] Multiple hydrogen-bond formation has been studied by NMR[2] and IR spectroscopy,[3] X-ray diffraction,[4] melting points,[5] or theoretical calculations.[6] In several previous works we have shown that base pairing can also be observed by UV/Vis spectroscopy if one of the complementary partners contains a chromophore, which is characteristically influenced by hydrogen bond formation.[7]

Barbituric acid (BA) derivatives are well-established as model receptors for studying multiple hydrogen-bond formations with nucleobase derivatives and related compounds.[3,8] BAs are readily available and can be chemically modified on demand.[9] For this purpose, barbiturate dyes have been constructed in such a way that the hydrogen bond formation affects the electron density of one of the substituent of the chromophore. Conceptually, an electron-withdrawing substituent such as the 4-nitrophenyl group or the 4-pyridinium ring is coupled at the five position of the six-membered BA ring.[7] As long as the BA exists in its keto form, those compounds are rarely coloured because the π-conjugation is interrupted by a sp^3-hybridised carbon atom. In contrast, the enol form of such BA dyes possesses a strong positive resonance effect and a push–pull chromophore results, which features an intense UV/Vis absorption band (Scheme 1).

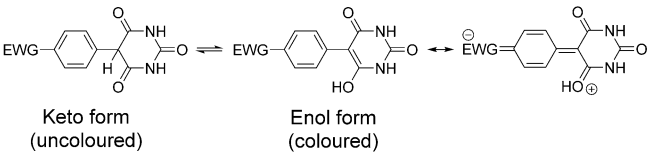

Scheme 1. Principle of induction in the push–pull system by keto-enol tautomerism of a barbiturate dye and resonance formulary of the enol form. EWG = electron withdrawing group.

However, several external influences can trigger the occurrence of the enol form. Supramolecular complex formation or common acid–base reaction can generate the enol or enolate form. Furthermore, the nature of solvents can have a fluctuating effect on that keto–enol equilibrium and thus the associated colour. If the precipitating agent will abstract the acidic proton of the BA, the overall HBA (hydrogen-bond-accepting) strength of the former ADA sequence is significantly enhanced. This effect was utilised by pyridinium-substituted barbiturate betaine dyes of the Reichardt-type,[7b] which showed optical response towards nucleobase derivatives via the anionically charged barbiturate moiety.[7b]

[a] *A. Schade, Dr. K. Schreiter, Prof. Dr. S. Spange*
Technische Universität Chemnitz, Department of Polymer Chemistry
09107 Chemnitz (Germany)
Fax: (+49) 371-531-21239
E-mail: stefan.spange@chemie.tu-chemnitz.de

[b] *Dr. T. Rüffer, Prof. Dr. H. Lang*
Technische Universität Chemnitz, Department of Inorganic Chemistry
09107 Chemnitz (Germany)

Supporting information for this article can be found under http://dx.doi.org/10.1002/chem.201504932.

Related studies were done with the enolizable chromophore 1-*n*-butyl-5-(4-nitrophenyl)barbituric acid (NPBA), which showed the complexity of this field.[7a] Unfortunately, the optically measured effects by UV/Vis spectroscopy, which are caused by supramolecular complex formation of NPBA, were not very significant. In this work, we will continue the study on chromophoric BA derivatives. The aim is to locate the way to detect optically any nucleobase by a colour change and determine crucial properties of the receptor dye, which are required to achieve this target.

Concerning this long-term objective, there is one important issue, which will be treated in this manuscript to complement the conceptual approach: Does an increased Brønsted acidity of the BA chromophore enhance the complex formation with a nucleobase derivative or does it gather preferentially the genuine salt formation? In this part, the anionically charged BA component will be operating on supramolecular complex formation.

An increased acceptor strength can be simply achieved by insertion of an additional nitro group in *ortho*-position of the phenyl ring of NPBA. Those compounds **4** are accessible by nucleophilic aromatic substitution of 2,4-dinitrofluoro-benzene with barbituric acid salts.[10] The mono *N*-alkyl substituted BA **4b** is beneficial to obtain a better solubility in nonpolar solvents.[7a,11] Additionally, the *n*-butyl group barricades one hydrogen-bonding sequence of the BA, thus solely a 1:1-complex formation can take place.[7a,c]

As a second chromophore with weaker acidity, 5-(4-((1,3-dioxo-1*H*-inden-2(3*H*)-ylidene)methyl)phenyl)barbituric acid derivatives **7b**,**c** have been chosen (Scheme 2). Compounds of type **7** possess a larger conjugated π-system and show a longer wavelength UV/Vis absorption band and a weaker acidity than **4** or NPBA.

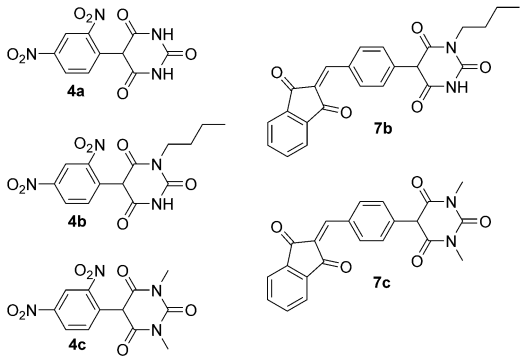

Scheme 2. Molecular structures of the five barbituric acid dyes **4a**–**c** and **7b**,**c** that were used in this study.

The *N*,*N*-dialkylated derivatives **4c** and **7c** (Scheme 2) were used as reference chromophores to study the genuine salt formation, because both hydrogen bonding sequences are blocked. Therefore, the UV/Vis spectroscopic respond is preferentially related to an acid–base reaction of the chromophore with a nucleobase derivative or a related compound.[12]

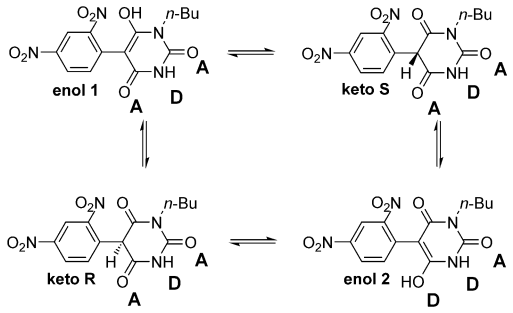

Scheme 3. Keto–enol tautomerism of 1-*n*-butyl-5-(2,4-dinitrophenyl)barbituric acid (**4b**). The resulting hydrogen bonding sequence pattern (A = H-bond acceptor, D = H-bond donor) for each tautomer is indicated.

The expected tautomeric species among the keto–enol equilibria of 1-*n*-butyl-5-(2,4-dinitrophenyl)-barbituric acid (**4b**) are shown in Scheme 3.

Optical properties of the enolizable barbituric acid dyes **4a**–**c**, **7b**, and **7c** are measured in a set of 36 various organic solvents and twelve ionic liquids to investigate the solvatochromism of the dyes as function of various solvent properties. Goal of this specific work is to obtain quantitative information about the effect of the environments HBD (hydrogen-bond-donating), HBA (hydrogen-bond-accepting), and dipolarity/polarizability properties on the shift of the UV/Vis absorption band of the dyes by using the linear solvation energy (LSE) relationships of Kamlet–Taft[13] and Catalán,[14] respectively. This solvatochromic method was applied for investigations of several solvatochromic dyes of the BA type and others.[7b,15]

Brønsted acid strength of the dyes has been measured by common acid–base titration and the results have been evaluated by means of the established Henderson–Hasselbalch equation (HHE) according to our previous study.[7a]

According to our previous studies,[7a,b,11] the nucleobase derivatives 1-*n*-butylthymine (BuTy), 9-ethyladenine (EtAd), 1-*n*-butylcytosine (BuCy), and 9-ethylguanine (EtGu), and 2,6-diacetamidopyridine (DACP) were used as receptors (Scheme 4) to study the base pairing effect.

Complex formations of **4b**,**c** and **7b**,**c**, respectively, with the different receptors of Scheme 4 were studied by means of UV/Vis and NMR titration experiments. Solid-state structures were examined using X-ray structure analyses of suitable crystals of BAs and their available adducts with nucleobase derivatives.

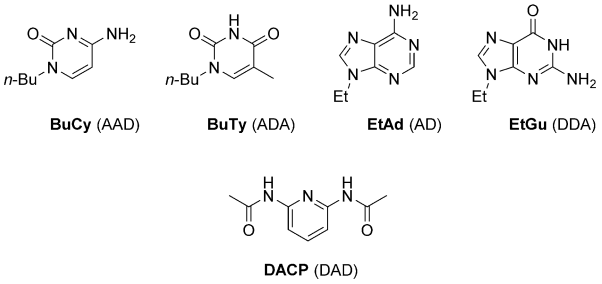

Scheme 4. Receptors and their hydrogen-bonding sequences (A = H-bond acceptor, D = H-bond donor) used in this work.

Results and Discussion

Synthesis

The synthetic procedure for dyes **4a–c** is shown in Scheme 5 and for dyes **7b,c** in Scheme 6. A detailed procedure is given in the Experimental Section.

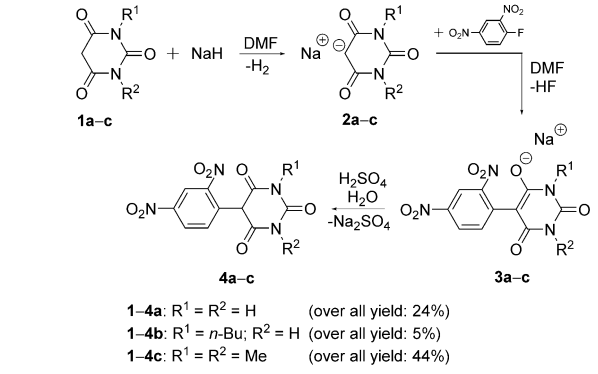

Scheme 5. Synthesis route for 5-(2,4-dinitrophenyl)barbituric acids **4a–c**.

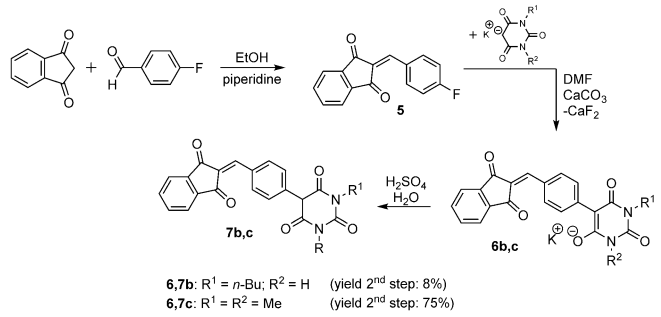

Scheme 6. Synthesis of 5-(4-((1,3-dioxo-1*H*-inden-2(3*H*)-ylidene)methyl) phenyl)barbituric acids (**7b,c**).

The barbituric acid 5-(4-((1,3-dioxo-1*H*-inden-2(3*H*)-ylidene)-methyl)phenyl) derivatives **7b,c** were synthesised utilising nucleophilic aromatic substitution of the corresponding fluoro compound (**5**), which is accessible by a Knoevenagel condensation reaction. Mentionable for a successful reaction is the use of $CaCO_3$ to trap the generated fluoride anion completely. Otherwise, the fluoride anion is able to catalyse the retro-Knoevenagel condensation, which has a negative impact on the overall yield.

In spite of the low yield in several cases, by reason of the simple procedure the products can be easily separated from the reactants.

Structure of 4a and 4c in the solid state

Compound **4a** crystallises from an ethanol/CH_2Cl_2 mixture within the triclinic space group $P\bar{1}$. Two crystallographically different molecules of **4a** in two different conformations were obtained; one has the enol group on the side of the *ortho*-nitro group, and one has the enol group on the opposite side (Scheme 3) in the asymmetric unit together with two ethanol solvent molecules (Figure 1). The carbon atoms C8 and C18 of solid **4a** are sp^2-hybridised, as revealed by the sum of their bond angles of 359.9(3)/359.9(3)° for C8/C18 (Figure 1). Consequently, the hydrogen atoms were found as enol species at the oxygen atoms O6 and O13, interacting as hydrogen bond donors with ethanol molecules (Scheme 7; Supporting Information, Figure S29). The different C–C and C–O bond lengths at the C7/C9 and C17/C19 atoms of the barbituric acid (Figure 1) validate the formation of an enol species.

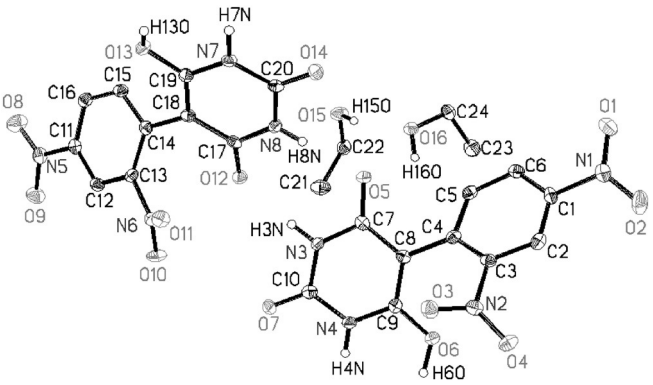

Figure 1. ORTEP (ellipsoids set at 50% probability) of the asymmetric unit of **4a**. Selected bond lengths [Å] and angles [°]: C8–C4 1.474(2), C8–C7 1.437(2), C8–C9 1.375(2), C7–O5 1.241(2), C9–O6 1.321(2), C18–C14 1.472(2), C18–C17 1.432(2), C18–C19 1.372(2), C17–O12 1.244(2), C19–O13 1.324(2); C4-C8-C7 118.9(2), C4-C8-C9 122.9(2), C7-C8-C9 118.1(2), C14-C18-C17 120.2(1), C14-C18-C19 121.8(2), C17-C18-C19 117.9(2).

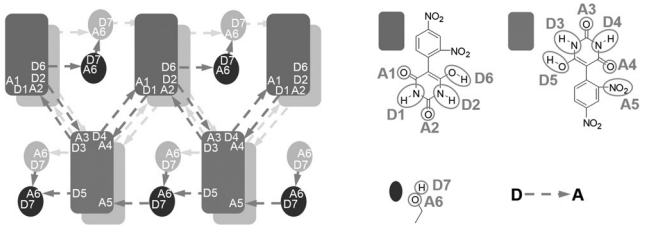

Scheme 7. Illustration of the two strands of **4a** within the crystallographic structure and their hydrogen bonds. Dark grey and grey squares represent the different conformation of **4a**, the grey ovals are ethanol molecules, the lighter squares and ovals belong to the strand in the back.

Molecules of **4a** form a chain along the crystallographic *c* axis, connected by two hydrogen bonds. Involved into these hydrogen bonds are the hydrogen bond donor groups N3–H3N, N4–H4N, N7–H7N, and N8–H8N as well as the hydrogen bond acceptors O5, O7, O12, and O14 (Figure 1). Two of such chains interact with each other by hydrogen bonds between two ethanol molecules. Both strands run in opposite directions and always the different conformational molecules lay next to each other (Scheme 7). These hydrogen bonded double-strands are connected further by π–π interactions, forming a 3D network (Figure S30).

Compound **4c** crystallises from a CH_2Cl_2/*n*-pentane mixture in the monoclinic space group $P2_1/c$. Importantly, **4c** forms

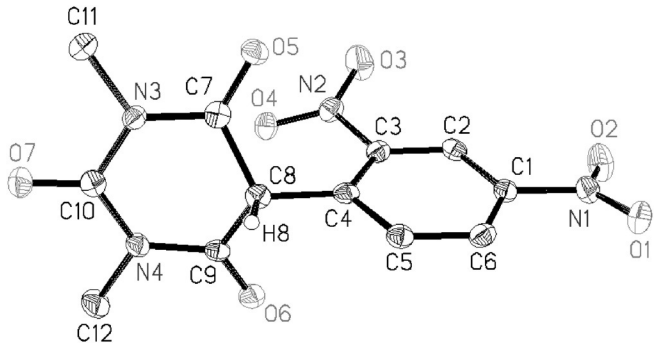

Figure 2. ORTEP (ellipsoids set at 50% probability) of the molecular structure of **4c**. Selected bond lengths [Å] and angles [°]: C8–C4 1.508(2), C8–C7 1.516(2), C8–C9 1.517(2), C7–O5 1.209(2), C9–O6 1.209(2); C4-C8-C7 114.7(1), C4-C8-C9 112.4(1), C7-C8-C9 113.5(1).

a ketobarbituric acid in the solid state (Figure 2) which is in contrast to **4a**. We point out that the carbon atom C8 is sp^3-hybridised with a sum of the bond angles of 340.6(2)°. Additionally, the bond lengths of the atoms C7/C9 to C8 are of equal distance (Figure 2).

Compound **4c** in the solid state is present as dimer, owing to an intermolecular π–π interaction between the *ortho*-nitro group and the phenyl ring of two different molecules (Figure S31).

These crystallographic studies show that depending on the substitution pattern and used solvents either the keto or enol tautomeric constitution occurs in the solid state.[16]

Acidity measurements in aqueous solution

The pK_a values for all of the compounds were determined by the HHE [Eq. (1)][17] in a mixture of water/methanol (ratio 5:1, v/v) at 20 °C by pH-dependent UV/Vis titration. The absorbance of the UV/Vis absorption maximum of the neutral, the mono-anionic, and the dianionic barbituric acids, respectively, were plotted as function of the pH [Eq. (2) and (3)]. The parent barbituric acid derivatives show UV/Vis absorption maxima at about 350 nm, and the mono-anionic form at about 400 nm. The dianions of barbituric acids **4a** or **4b** absorbs at about 440 nm in the respective media. The second deprotonation step of **4a** or **4b** takes place at the NH group, which is verified by the fact that the *N*,*N*-dialkylated derivative **4c** did not show this UV/Vis absorption band at 444 nm at pH > 11.

$$pK_a = pH - \log(c_{A^-}/c_{HA}) \quad (1)$$

$$pK_a\,(1) = pH - \log(A_{BS^-}/A_{BS}) \quad (2)$$

$$pK_a\,(2) = pH - \log(A_{BS^{2-}}/A_{BS^-}) \quad (3)$$

The obtained pK_a values are summarised in Table 1. Compared to NPBA (p$K_a \approx 2.0$),[7a] 5-phenylbarbituric acid (p$K_a = 2.54$)[18] and the parent BA (p$K_a = 4.02$),[18] **4a–c** are more acidic (p$K_a \approx 0.0$). The BA derivatives with an enlarged π-system (**7b,c**) are surprisingly more acidic than NPBA (p$K_a \approx 1.3$), but less acidic than **4a–c**. Detailed information as well as the UV/Vis absorption spectra of the titration experiments are given in the Supporting Information (Figures S16–S27).

Table 1. pK_a values of **4a–c** and **7b,c**.

	4a	4b	4c	7b	7c
pK_a (1)	0.14	0.13	−0.23	1.35	1.34
pK_a (2)	11.76	12.42	/	/[a]	/[a]

[a] Decolourisation at pH > 6 is due to base reacting with the benzylidene double bond.

Solvatochromic studies

The evaluation of the measured solvatochromic data ($\tilde{\nu}_{max}$) has been performed by LSE (linear solvation energy) relationships using either the Kamlet–Taft[13] [Eq. (4)] or the Catalán equation[14] [Eq. (5)].

$$\tilde{\nu}_{max} = \tilde{\nu}_{max,0} + a\alpha + b\beta + s\pi^* \quad (4)$$

$$\tilde{\nu}_{max} = \tilde{\nu}_{max,0} + a\mathrm{SA} + b\mathrm{SB} + d\mathrm{SP} + e\mathrm{SdP} \quad (5)$$

$\tilde{\nu}_{max}$ is the measured solvent dependent UV/Vis absorption maximum of a dye in a specific solvent. $\tilde{\nu}_{max,0}$ is the calculated UV/Vis absorption maximum of the solvent-unaffected dye, α is the HBD parameter, SA is the solvent acidity, which relates to α, β is the HBA parameter, SB is the solvent basicity, which relates to β, π* is the solvent dipolarity/polarizability parameter, SdP is the solvent dipolarity, and SP the solvent polarizability. *a*, *b*, and *s* as well as *d* and *e* are solvent-independent correlation coefficients. The advantage of the Catalán LSE relationship is that it considers the solvent polarizability and dipolarity as independent terms, whereas Kamlet–Tafts's π* is a blend of both.

Multiple square correlation analysis of $\tilde{\nu}_{max}$ of the dyes **4a–c** and **7b,c** measured in 36 organic solvents and twelve ILs with the empirical solvent parameters according to Equation (4), or (5) are performed to examine the correlation coefficients *a*, *b*, *s*, *d*, *e*.

Correlation coefficients of solvatochromic dyes determined from Eq. (4) and (5) deliver predictions on preferred solvation sites of the dye by a distinct property of the solvent. Thus, the knowledge of the coefficients allows a semi-quantitative interpretation on specific and nonspecific solvation of a solvatochromic molecule.[15b,h]

Recently, SP and SdP parameters of ILs were firstly determined by our group.[19] Hence, we are specifically interested in the application of these SP and SdP parameters of IL for interpretation of solvatochromic data to show their reliability.

The UV/Vis spectra of compounds **4a–c** and **7b,c** were measured in 36 various organic solvents and compounds **4a–c** additionally in twelve ILs. The UV/Vis absorption maxima of **4a–c** and **7b,c** or their deprotonated species **4a$^\theta$–c$^\theta$** and **7b$^\theta$,c$^\theta$** are presented in the Supporting Information, Table S2 and S3. The Kamlet–Taft and Catalán empirical solvent parameters for

these solvents were taken from previous reports and are given in the Supporting Information, Table S1.

Representative UV/Vis spectra of **4b**$^{\theta}$ measured in six solvents are shown in Figure 3 and in six ILs in Figure 4.

For all of the compounds, the largest hypsochromic shift was measured in the most acidic solvent used, 1,1,1,3,3,3-hexafluoro-2-propanol (HFIP), and the largest bathochromic shift in the most basic solvent used, hexamethylphosphoric triamide (HMPA). The solvatochromic range $\Delta\tilde{\nu}$ [$\Delta\tilde{\nu}=\tilde{\nu}$ (HFIP)$-\tilde{\nu}$ (HMPA)] of these compounds amounts to 5110 cm^{-1} for **4c**$^{\theta}$, 5840 cm^{-1} for **4b**$^{\theta}$, and 7600 cm^{-1} for **4a**$^{\theta}$.

The concentration of the dye is very low ($c=5\times10^{-5}$ mol L^{-1}). Thus the solvent is existent in about 100 000-fold excess to the dye. Therefore, also a weak base with p$K_a<2$ at 10^{-4} mol L^{-1} becomes partly protonated, for example, ethanol (pK_a $C_2H_5OH_2^+=-2.4$). This can be estimated by applying the acid base equilibrium equation but it is not clear which number of solvent molecules are involved on the molecular level.

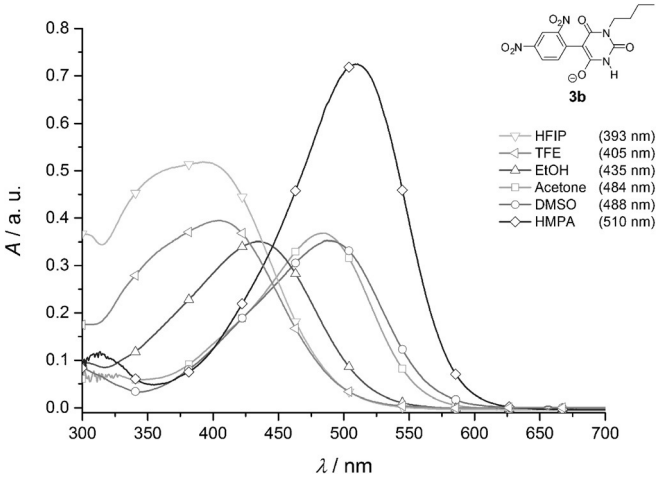

Figure 3. UV/Vis spectra of **4b**$^{\theta}$ in six different solvents (HFIP: 1,1,1,3,3,3-hexafluoro-2-propanol; TFE: 1,1,1-trifluoroethanol; EtOH: ethanol; DMSO: dimethylsulfoxide; HMPA: hexamethylphosphoric triamide).

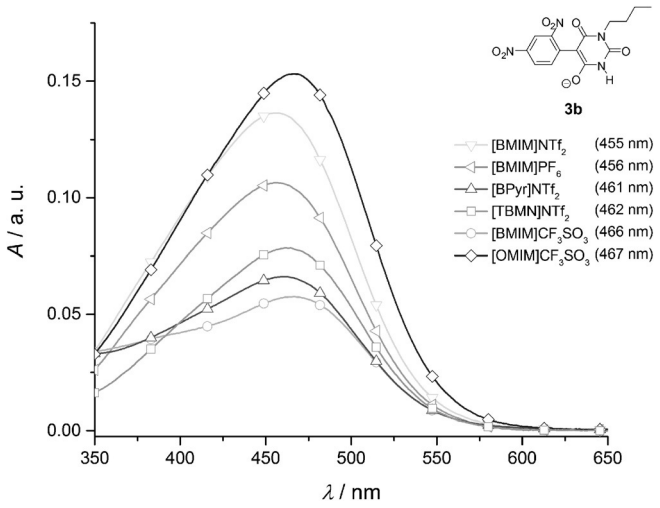

Figure 4. UV/Vis spectra of **4b**$^{\theta}$ in six ionic liquids. [BMIM] = 1-butyl-3-methylimidazolium; [OMIM] = 1-octyl-3-methylimidazolium; [BPyr] = 1-butylpyridinium; [TBMN] = tributylmethylammonium; NTf_2 = bis(trifluoromethylsulfonyl)imide.

This issue must be considered to understand the measured effects of the solvent upon the position of the UV/Vis absorption band. If the solvent shell serves as base medium, a proton is abstracted from the dye and the anionic form is observed. This feature occurs when the dye is measured in solvents possessing moderate and strong hydrogen-bond-accepting (HBA) properties. Hence, the dissolution process of **4a–c** in such solvents is associated with an acidochromic process. Whether the anionic shape of the dye (**4a**$^{\theta}$–**c**$^{\theta}$) is released in any solvent instead of **4a–c**. This can be easily tested when the strong base DBU (1,8-diazabicyclo[5.4.0]undec-7-ene) (pK_a DBU-H$^+$ = 12.0) is added in a small portion ($c_{DBU}=c_{dye}$) to the dye solution. If the UV/Vis absorption band of the dissolved dye is not affected by DBU traces, the anionic form is already present. Due to the position of UV/Vis absorption, bands of anionic dyes are also solvent-dependent,[15a] the DBU test is necessary to ensure the behaviour of the dye in those solvents, which are very weak bases. Thus, in the following classes of solvents the dye is present in its anionic form: aliphatic alcohols, amides, ketones, carbonic acid ester, amines, and ionic liquids.

It is observable that even in the strong HBD solvent 1,1,1,3,3,3-hexafluoro-2-propanol (HFIP), the anionic form is formed, as shown by the fact that DBU addition does not affect the UV/Vis absorption maximum in this solvent. Furthermore, in alcoholic solvents the dyes show an asymmetric UV/Vis absorption band, which indicates that the solvation of the enolate species seems manifold. Consistently the longest UV/Vis absorption band has been used in the multiple square correlation analyses for the evaluation of Equations (4) and (5).

The keto form of the dye is only present in few solvents, such as halogenoalkanes (alkyl halides). Therefore, a colourless or pale-yellow-coloured ($\lambda_{max}<300$ nm) solution is observed.

Usually, for the multiple square correlation analyses of $\tilde{\nu}_{max}$ as function of SA, SB, SP, and SdP (or α, β, and π^*) these solvents have to be excluded where a chemical alteration of the dye takes place.

The results of the multiple square correlation analyses are compiled in Table 2. Graphically depicted results were given in Figure 5 and the Supporting Information (Figures S1–S3).

Altogether, the calculated coefficient *a* shows a positive algebraic sign for the compounds studied, which indicates a hypsochomic effect with increasing acidity of the solvent (α or SA). This result indicates the preferred solvation of the barbiturate anion in acidic solvents. This explanation is in agreement with solvatochromic phenomena of established betaine dyes such as Reichardt's dye[14h] or other negatively charged dyes.[15a]

The positive solvatochromic effect of the HBA ability of the solvents ($b<0$) results from the interactions of the NH groups of the BA anion with an electron lone pair of the solvent. With increasing the number of *N*-alkylation sites, the *b* coefficient decreases:

b from Kamlet–Taft: -1.397 (**4a**$^{\theta}$)$\rightarrow-0.732$ (**4b**$^{\theta}$)$\rightarrow-0.434$ (**4c**$^{\theta}$)

b from Catalán: -0.792 (**4a**$^{\theta}$)$\rightarrow-0.493$ (**4b**$^{\theta}$)$\rightarrow\pm0.000$ (**4c**$^{\theta}$)

Table 2. Calculated solvent-independent correlation coefficients *a*, *b*, and *s* according to the Kamlet–Taft Equation (4) and *a*, *b*, *d*, and *e* of the Catalán Equation (5) for the solvatochromic response of **4a–c**.[a]

		4a$^{\theta}$	**4b**$^{\theta}$	**4c**$^{\theta}$
Kamlet–Taft Equation (4)	$\tilde{\nu}_{max,0}$	23.042	22.330	22.217
	a	2.662	2.305	2.171
	b	−1.397	−0.732	−0.434
	s	−1.869	−1.553	−1.754
	n	32	30	33
	sd	0.310	0.323	0.307
	r	0.98	0.97	0.97
	f	≤0.0001	≤0.0001	≤0.0001
Catalán Equation (5)	$\tilde{\nu}_{max,0}$	26.863	25.508	25.371
	a	4.478	4.266	3.886
	b	−0.792	−0.493	±0.000
	d	−4.529	−3.137	−4.124
	e	−2.574	−2.561	−1.949
	n	30	28	31
	sd	0.315	0.294	0.200
	r	0.97	0.97	0.98
	f	≤0.0001	≤0.0001	≤0.0001

[a] Owing to the anionic form is generated in the solvents, **4a**$^{\theta}$**–c**$^{\theta}$ are observed in reality. Additionally, given is the correlation coefficient *r*, the standard deviation *sd*, the number of solvents *n* and the significance *f*.

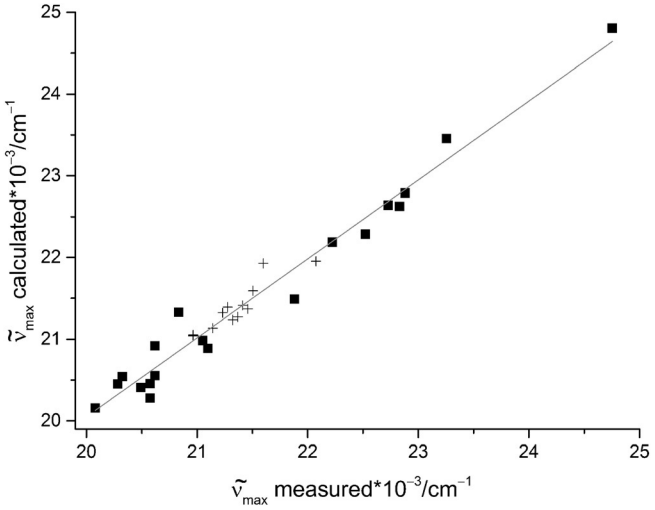

Figure 5. Calculated UV/Vis absorption maxima of compound **4c**$^{\theta}$ by Catalán Equation (5) with coefficients from Table 2 versus measured UV/Vis absorption maxima in a set of 19 organic solvents (■) and 12 ILs (+).

This result shows that even the anionic form is able to interact with a donor solvent, which is measurable by the solvatochromic response and it is of importance to understand the supramolecular complex formation of the anionic forms of barbiturates, which will be discussed below.

Despite the negative charge of the BA anion, which contains NH moieties, these NH groups are still able to interact with further HBA sites. Apparently, electrostatic repulsion is clearly overcompensated by the NH···HBA interaction strength.

The negative algebraic sign of *s* indicates a stronger solvation of the first exited state with increasing polarity of the solvents. Thus, the first excited state is more dipolar than the electronic ground state. This result is well-known for chromophores with a neutral ground state and a polar first exited state, such as nitroaniline derivatives.[20] A related result was found for anionic thiazole based chromophores with a nitro group as acceptor moiety.[15a]

With the help of the Catalán Equation (5), the influence of polarizability and dipolarity on shift of $\tilde{\nu}_{max}$ can be separately quantified. Both coefficients are negative indicating a bathochromic shift with increased polarizability ($d<0$) as well as dipolarity ($e<0$).

The polarizability of the solvent influences the UV/Vis absorption maximum of these dyes two times more than the dipolarity. This d/e ratio matches their contributions to the π* parameter[14h] and agrees with the results from the Kamlet–Taft correlations.

The ILs fit well in the correlation plot among the organic solvents, which is shown in Figure 5 for the solvatochromism of **4c**$^{\theta}$.

This result shows that the empirical solvent parameters SP and SdP of ILs[19] can be readily applied to interpret solvatochromic effects in comparison to organic solvents.

A correlation of $\tilde{\nu}_{max,3b}$ versus $E_T(30)$ shows a moderately good correlation (Supporting Information, Figure S6), because both dyes show a strong hypsochromic effect caused by acidic solvents ($a>0$).[14h] They behave different by the effect of polarizability and dipolarity of solvents. The anionic barbiturate dyes **4a**$^{\theta}$**–c**$^{\theta}$ show a bathochromic shift of the UV/Vis absorption maximum as function of $\tilde{\nu}_{max}$ in contrast to Reichardt's $E_T(30)$ dye, which shows a hypsochromic shift of the UV/Vis absorption maximum with increased dipolarity/polarizability of the solvent.

The UV/Vis absorption spectra of the chromophoric dyes **7b** and **7c** were also measured within various organic solvents (Supporting Information, Table S3). The solvatochromic range $\Delta\tilde{\nu}$ of these compounds amounts to 6420 cm^{-1} for **7b** (HFIP to HMPA) and 6700 cm^{-1} for **7c** (HFIP to HMPA). The results of the multiple square correlation analyses of $\tilde{\nu}_{max}$ with the solvent parameters are given in Table 3 and in the Supporting Information (Figures S4 and S5).

Both dyes show a strong hypsochromic UV/Vis shift with increased solvent acidity ($a>0$). This effect is similar to the results of chromophores **4a–c** and also indicates a deprotonation of the chromophores during dissolution of **7b,c**. The hypsochromic shift of the UV/Vis absorption maximum results from the interaction of HBD solvents with the anionic barbiturate unit. The UV/Vis absorption maxima did not change after addition of DBU, indicating that the anionic forms **7b**$^{\theta}$**,c**$^{\theta}$ were already present.

A bathochromic shift of the UV/Vis absorption maximum was found for **7b**$^{\theta}$ with increasing SB of the solvent, because of the interaction by HBA solvents with the NH function. The solvatochromic shift of the chromophore **7c**$^{\theta}$ shows no dependence on the properties of HBA solvents, which is caused by the alkylation of both NH functionalities.

Unspecific interactions (SP, SdP, or π*) cause a bathochromic shift of $\tilde{\nu}_{max}$ of **7b**$^{\theta}$**,c**$^{\theta}$, comparable with the effect observed for **4a**$^{\theta}$**–c**$^{\theta}$. An exception is the correlation of solvatochromism of

Table 3. Solvent-independent correlation coefficients *a*, *b* and *s* according to the Kamlet–Taft Equation (4) and *a*, *b*, *d* and *e* of the Catalán Equation (5) for the solvatochromic response of **7b** and **7c**.[a]

		7b$^{\theta}$	**7c**$^{\theta}$
Kamlet–Taft Equation (4)	$\tilde{\nu}_{max,0}$	19.470	17.702
	a	2.452	3.057
	b	−1.467	±0.000
	s	−0.978	±0.000
	n	21	20
	sd	0.323	0.348
	r	0.98	0.97
	f	≤0.0001	≤0.0001
Catalán Equation (5)	$\tilde{\nu}_{max,0}$	21.815	20.927
	a	4.795	4.997
	b	−0.836	±0.000
	d	−2.894	−3.171
	e	−1.694	−0.979
	n	20	20
	sd	0.226	0.265
	r	0.99	0.99
	f	≤0.0001	≤0.0001

[a] Since the anionic form is generated in the solvents, **7b**$^{\theta}$ and **7c**$^{\theta}$ are observed in reality. Also given is the correlation coefficient *r*, the standard deviation *sd*, the number of solvents *n*, and the significance *f*.

chromophore **7c**$^{\theta}$ explained by the Kamlet–Taft Equation (4), which apparently shows no dependence on π^*.

Exemplary, the solvatochromic ranges $\Delta\tilde{\nu} = 7600\ cm^{-1}$ for **4a**$^{\theta}$ and $\Delta\tilde{\nu} = 6700\ cm^{-1}$ for **7c**$^{\theta}$ are pretty large compared to those of established solvatochromic dyes.[8d] It should be distinguished whether a positive or negative solvatochromic dye is to consider to equitably evaluate the dimension of the solvatochromic shift.[8c,21] Positive solvatochromism of a dye is clearly defined. It means that the longest wavelength UV/Vis absorption shifts bathochromically with increasing solvent polarity. That would be valid for the effect of dipolarity/polarizability of the solvent on $\tilde{\nu}_{max}$ of **4a**$^{\theta}$–**c**$^{\theta}$, **7b**$^{\theta}$,**c**$^{\theta}$ and also for 5-(4-nitrophenyl)barbituric acid derivatives in the previous work.[7a] That is because the algebraic signs of coefficients *s* from Equation (4) and *d* and *e* from Equation (5) are negative.

Opposing to the effect of dipolarity/polarizability, the UV/Vis absorption bands of **4a**$^{\theta}$–**c**$^{\theta}$, **7b**$^{\theta}$,**c**$^{\theta}$ and for the 5-(4-nitrophenyl)barbituric acid derivatives[7a] are hypsochromically shifted with increasing HBD strength (α) or acidity of the solvent (SA). That result would suggest negative solvatochromism with respect to α or SA. Thus the dyes **4a**$^{\theta}$–**c**$^{\theta}$, **7b**$^{\theta}$,**c**$^{\theta}$ and the 5-(4-nitrophenyl)barbituric acid derivatives[7a] are not absolute positive solvatochromic dyes in spite of the negative algebraic signs for the *s*, [Eq. (4)] or *d* and *e* [Eq. (5)] coefficients.

Table 4 shows a comparison of the solvatochromic properties of three classes of barbiturate dyes from previous reports and this work with respect to the solvatochromic range and a classification as to whether positive or negative solvatochromism is determined.

The facts of Table 4 clearly indicate a positive solvatochromism for BA dyes of the merocyanine type[9b,15d,h] because *a*, *s*, *d* and *e* coefficients from Equations (4) and (5) altogether show a negative algebraic sign. Likewise, pyridinium-betaine dyes of the Reichardt-type, which contain the BA moiety anion as negative part, unambiguously show a negative solvatochromic property because *a*, *s*, *d* and *e* coefficients from Equations (4) and (5) altogether show a positive algebraic sign.[7b]

Table 4. Comparison of the solvatochromic properties of the BA dyes **4a**$^{<gq>}$–**c**$^{\theta}$; **7b**$^{\theta}$,**c**$^{\theta}$ with negative[7b] and positive solvatochromic[15d] BA dyes.[a]

	$^{-}$BA–EWG^{+} betaine dyes[7b]	BA=EWG merocyanine dyes[15d]	$^{-}$BA–EWG this work
algebraic sign of *s* from Eq. (4) and *d*, *e* from Eq. (5)	+	−	−
algebraic sign of *a* from Eq. (4) and (5)	+	−	+
solvatochromic range $\Delta\tilde{\nu}$ [cm^{-1}]	ca. 10000	<4500	5100–7600

[a] EWG = electron withdrawing group, EDG = electron donating group.

If the original definition would be applied, the dyes **4a**$^{\theta}$–**c**$^{\theta}$, **7b**$^{\theta}$,**c**$^{\theta}$ would ostensibly show world records in positive solvatochromism despite the fact that the large solvatochromic range is actually caused by the HBD solvation rather than by the "polarity".

Thus, non-critical use of original definitions for positive or negative solvatochromism makes no sense for these types of solvatochromic dyes (for related solvatochromism of anionic dyes see also Ref. [15a,g]). This actuality instructive demonstrates the usefulness of LSE correlation analyses for interpretation of solvatochromic effects.

Despite this difficulty of classification, the barbiturate dyes **4a**$^{\theta}$–**c**$^{\theta}$, **7b**$^{\theta}$,**c**$^{\theta}$ definitively show genuine solvatochromism in most of the solvents because all $\tilde{\nu}_{max}$ data of alcohols fit well in the correlation equations (Figure 5). Acidochromism would only happen if the keto form of barbiturate dyes were treated in CH_2Cl_2 (or another halogenoalkane) with a base. This circumstance must be considered by interpretation the titration experiments of the dyes with the receptor molecules.

Complex formation studies

The interactions of **4b** and **7b**, respectively, with the different receptors were also investigated (Scheme 4). The titration experiments were carried out in CH_2Cl_2 for the pyridine derivative DACP and in a mixture of CH_2Cl_2/MeOH (ratio 25:1, v/v) for the nucleobase derivatives. The methanol addition was necessary because of the poor solubility of reactants and products in CH_2Cl_2.

The competition between complexation and salt formation was investigated by reference experiments of the receptors with **4c** and **7c**. As already mentioned, these compounds are not suited for supramolecular complex formation, because both hydrogen bonding sequences are barricaded by methyl substitution. Therefore, UV/Vis spectroscopic changes of **4c** and **7c** with the receptors can only be an effect of genuine salt formation. Complex formation of dye **4a** was not investi-

gated in this study, because of its poor solubility and the expected effects due to the present NH groups.

1-n-Butylcytosine

This nucleobase derivative has been used as model compound for study the competition between complexation and genuine salt formation, because of its complementary hydrogen bonding sequence to the enol 2 form of **4b** (Scheme 8). 1-*n*-Butylcytosine (BuCy) is also the most basic nucleobase derivative ($pK_a = 4.60$).[22]

The UV/Vis spectroscopic complex titration (Figure 6) was analysed by Equation (6), where ΔA is the difference of the absorbance at the UV/Vis absorption maximum and the absorbance of the stock solution, [S] is the concentration of the used chromophore, K_A is the association constant, e_1 is the obtained extinction coefficient of the complex, [L] is the concentration of the added receptor and b is the path length of the beam through the material sample of the immersion vessel.[12]

$$\Delta A = ([S]\, K_A\, e_1\, [L])/(1 + K_A\, [L])\, b \qquad (6)$$

The UV/Vis absorption intensity of **4b** at 451 nm increases with BuCy concentration. An association constant of 7220 ± 190 L mol^{-1} was calculated from Equation (7) (Supporting Information, Table S4). The bathochromically shifted UV/Vis absorption maximum (451 nm) hints at salt formation.

A second hypsochromic UV/Vis absorption maximum was found for **4b** at lower concentrations of BuCy. If the concentration of BuCy exceeds the concentration of **4b**, the intensity of the new bathochromic UV/Vis absorption band at 451 nm further increases, while the hypsochromic band is decreasing.

Isosbestic points are observed at 310 nm and 394 nm, which indicate that above a BuCy concentration of 2.047×10^{-4} mol L^{-1} only two chromophoric species are involved (Figure 6). At lower BuCy concentrations, the UV/Vis absorbance at 348 nm increases without appearing of an isosbestic point because of the keto–enol equilibrium. The UV/Vis absorption maximum at 348 nm shifts bathochromically with increased BuCy concentration. This hints at a complexation of the enol 2-form (Scheme 3), which is further deprotonated with increased BuCy concentration (Scheme 8).

To achieve a secure interpretation, separation of the UV/Vis absorption spectra into two separate Gauss functions with Origin Pro 9.1 g was employed (Figure 7). The UV/Vis absorption maximum at 468 nm belongs to the anionic form. The hypsochromic UV/Vis absorption maximum shift bathochromically. This indicates an interaction of the enol 2 form of **4b** with BuCy.

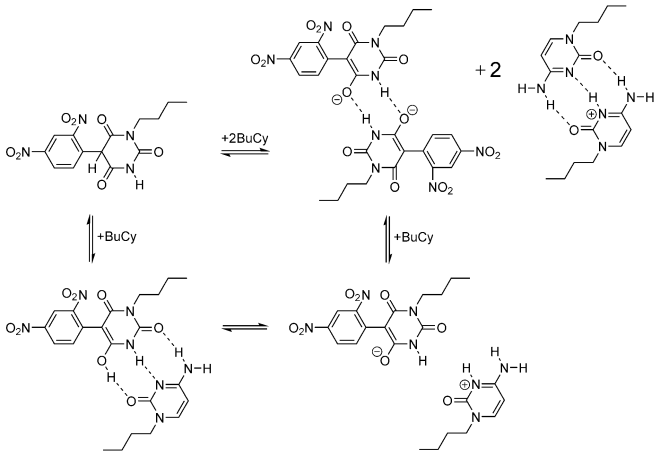

Scheme 8. Suggested competition between complexation and genuine salt formation of **4b** with BuCy.

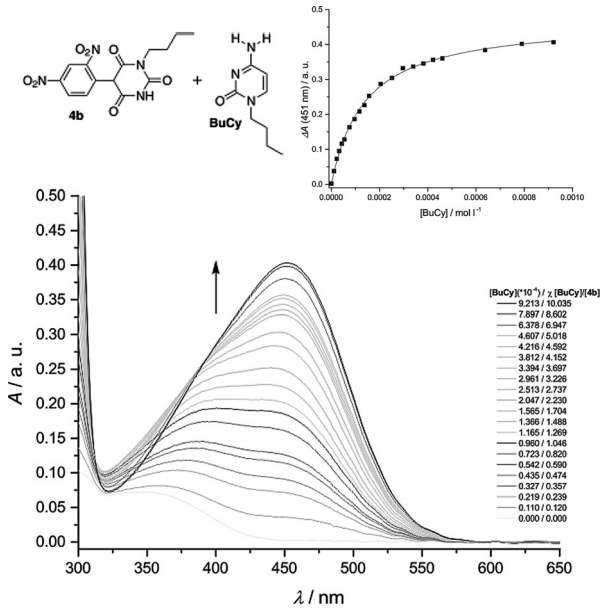

Figure 6. UV/Vis titration of **4b** [$c = 9.181 \cdot 10^{-5}$ mol l^{-1}] with BuCy in a mixture of CH_2Cl_2/MeOH (ratio 25:1, v/v).

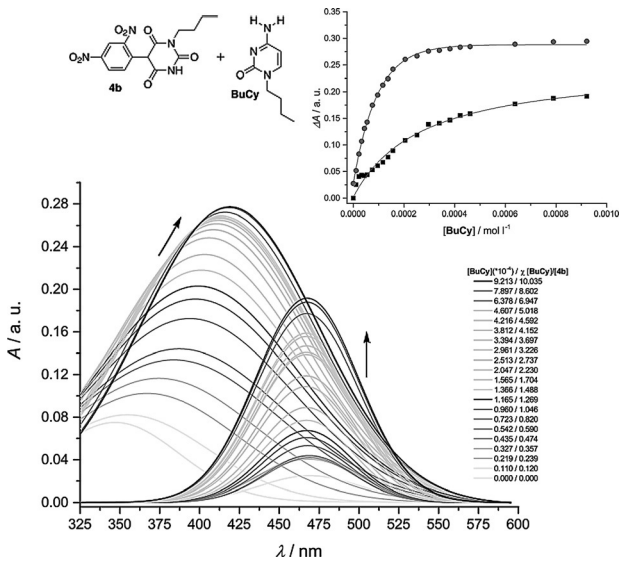

Figure 7. Separated UV/Vis absorption spectra of **4b** with BuCy in a mixture of CH_2Cl_2/MeOH (ratio 25:1, v/v).

Two association constants can be determined, the first for the UV/Vis absorption at 419 nm with $K_A(2) = 10750 \pm 240\ L\,mol^{-1}$ and the second for the UV/Vis absorption at 468 nm with $K_A(1) = 3670 \pm 360\ L\,mol^{-1}$. The higher association constant $K_A(2)$ shows that the complex formation is preferred against the genuine salt formation.

Dye **7b** absorbs at 345 nm in a mixture of CH_2Cl_2/MeOH (ratio 25:1 v/v), the UV/Vis absorption maximum of which is assigned to the keto form. By addition of BuCy to **7b**, the keto–enol equilibrium shifts towards the enol form (431 nm). This occurrence is optically detectable by a decrease of the UV/Vis absorption band at 345 nm, while the new UV/Vis absorption band at 431 nm increases. The UV/Vis absorption band at 431 nm contains a bathochromic shoulder at lower concentrations of BuCy. At higher concentrations of BuCy, a second UV/Vis absorption maximum at 513 nm occurs. This UV/Vis absorption band becomes dominant at higher concentrations of BuCy and belongs to the enolate species (Figure 8). The obtained association constants show a preferred interaction of BuCy with the enol form of **7b** ($K_A = 9070 \pm 530\ L\,mol^{-1}$). Genuine salt formation occurs again, but because of the lower acidity of compound **7b**, it is less dominant ($K_A = 1925 \pm 16\ L\,mol^{-1}$). These results confirm the hypothesis that a complementary hydrogen bonding sequence does influence the keto–enol tautomerism, which induces an optical response.

Compared to **4b**, the association constant between BuCy and **7b** is slightly decreased ($K_A(2)$ (**4b**) $= 10750\ L\,mol^{-1}$; $K_A(2)$ (**7b**) $= 9070\ L\,mol^{-1}$; Supporting Information, Table S6), which is caused by the decreased acidity of the enolic proton compared to **4b**. The found association constants for genuine salt formation K_A(**7b**) $= 1925\ L\,mol^{-1}$, decreases dramatically compared to K_A(**4b**) $= 7220\ L\,mol^{-1}$.

It could be shown that the lower acidity of **7b** compared to **4b** reduces the concurrence of genuine salt formation and the complexation becomes dominant, although the association constant between the BA and BuCy decreases slightly.

NMR titration experiments were performed to support the results from UV/Vis measurements. The ^{1}H NMR titration of **4b** with BuCy in CD_2Cl_2 also shows salt formation. The signal of the C5 hydrogen (5 ppm) at the barbituric acid keto form disappears with increasing BuCy concentration. Accordingly, a new signal appears at 14 ppm, which can be assigned to the protonation at BuCy. With increased BuCy concentration (excess to **4b**) this signal is upfield-shifted, because of the distribution of the positive charge over more than one BuCy molecule (Supporting Information, Figure S13). Additionally, both NMR signals of the H atoms at the five and six position of BuCy show the expected shift to lower field indicating a reduced electron density. The NMR titration experiment of BuCy with 1,1,1-trifluoroacetic acid was used to support the interpretation. The ^{1}H NMR spectrum shows signals of BuCy with a similar chemical shift, which indicates that during both titrations a protonation of BuCy occurs (Supporting Information, Figure S14).

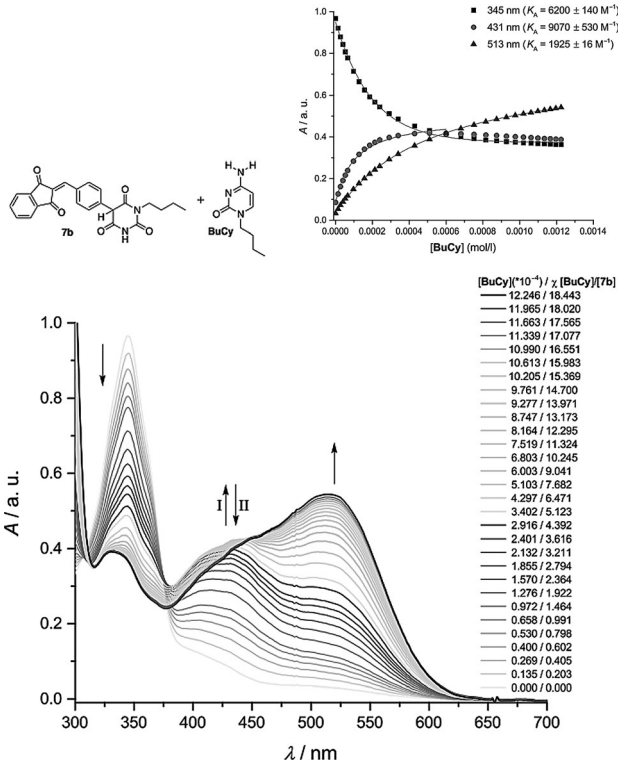

Figure 8. UV/Vis titration of **7b** ($c = 6.640 \cdot 10^{-5}\ mol\,L^{-1}$) with BuCy in a mixture of CH_2Cl_2/MeOH (ratio 25:1, v/v). UV/Vis absorption maximum at 345 nm (keto form) decreases; absorption maximum at 431 nm (enol form) increases (I) but at higher concentrations it decreases again (II); absorption maximum (enolate form) increases at 513 nm.

Structure of 4b/BuCy in the solid state

Deep-red crystals suitable for single-crystal X-ray diffraction studies were obtained by crystallisation of a 1:1 mixture of **4b** with BuCy from CH_2Cl_2/*n*-pentane at ambient temperature. **4b**/BuCy crystallises in the triclinic space group $P\bar{1}$. The structure of the asymmetric unit is given in the Supporting Information (Figure S34) together with selected bond lengths and angles. The deep-red colour of the crystals already indicate the formation of a barbiturate anion. Indeed, the asymmetric unit of **4b**/BuCy comprises mono-deprotonated **4b** (the barbiturate anion denoted further as **4b**$^{\theta}$), two crystallographically independent molecules of BuCy, of which each second is mono-protonated, and one water molecule. The presence of **4b**$^{\theta}$ is indicated by the sp^2-hybridised atom C8, as the sum of its bond angles is 360.1(10). Additionally, in case of **4a** this compound has been described as an enol-barbituric acid, as the bond lengths of C8 to C7 and C9 are significantly different (Figure 1). In case of **4b**$^{\theta}$, however, the C8–C7 and C8–C9 bond lengths are equal (Supporting Information, Figure S34) and consequently this molecule does not correspond to an enol-barbituric acid as **4a**. Instead, the barbiturate anion is detected.

The two crystallographically independent molecules of BuCy were taken as being each half-protonated (see above). This is revealed by the presence of dimers of the form $[(BuCy)_2H]^+$ in the solid state for each individual BuCy molecule (Figure 9). For example, the BuCy molecule with the atom N9 narrows to a further N9-carrying BuCy molecule with an N9$\cdots$N9A distance of 2.835 Å (Figure 9). Such a short distance is characteristic for

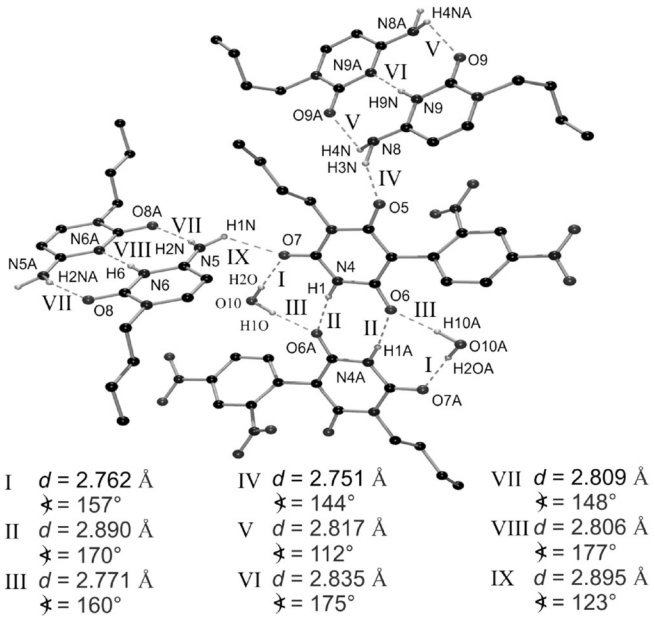

Figure 9. Selected part of the crystal structure of **4b**/BuCy. Grey dotted lines indicate intermolecular hydrogen bonds of type I–IX, with *d* giving the D···A distance and ∢ the D–H···A angle. All C-bonded hydrogen atoms are omitted for clarity.

an intermolecular hydrogen bond and thus only one N9 atom could be protonated. Related cytosine/cytosine-H^+-dimers have already been described.[23]

In the solid state, **4b**/BuCy molecules form a 3D network. The network contains of BA anion dimers are connected by two hydrogen bonds, which also interact with two water molecules (Figure 9). The two structurally different dimers of $[(BuCy)_2H]^+$ were stabilised by three hydrogen bonds (V and VI, VII and VIII; Figure 9). Additionally, they form hydrogen bonds with the BA anion dimers (IV, IX; Figure 9). One $[(BuCy)_2H]^+$ building block links the barbiturate dimers along the crystallographic *c* axis, the other along the crystallographic *b* axis (Figure S35). The described hydrogen bonds form a 2D layer, and π–π-interactions connect these layers along the crystallographic *a* axis.

9-Ethyladenine

The nucleobase derivative 9-ethyladenine EtAd ($pK_a = 4.25$) is less basic than cytosine ($pK_a = 4.60$).[22] Therefore, a reduced tendency for salt formation is expected. Investigations on the complex formation between barbituric acid and nucleobase derivatives by Kyogoku showed that the complex formation of barbituric acid with adenine is the strongest of all nucleobase derivatives and additionally stronger than the natural pendant, thymine with adenine.[3]

The keto form of BA presents the same hydrogen bond sequence as thymine, namely the ADA pattern. Therefore, a complex formation of the keto form with thymine by two hydrogen bonds was expected. This type of complexation should not result in an UV/Vis spectroscopic response, because a complexation with the enol-2 form is not expected. Consequently, an increasing enol-1 form was found for the complex formation of 5-(4-nitrophenyl)barbituric acid with EtAd.[7a] An explanation for this behaviour has still not been ascertained.

The UV/Vis titration experiment of **4b** with EtAd is shown in the Supporting Information, Figure S8. The new UV/Vis absorption maximum is found at 441 nm. An association constant of $K_A = 970 \pm 50\ L\,mol^{-1}$ was calculated from Equation (6) (Supporting Information, Table S7). The lower association constant compared to BuCy, results of the lower basicity of the nucleobase derivative EtAd. Additionally, stabilisation of the enol-2 form at low concentrations was not found for this nucleobase derivative. The UV/Vis absorption maximum at 348 nm did not increase. The UV/Vis absorption maximum of **4b**/EtAd shifts 10 nm hypsochromically compared to the salt formation with BuCy or DBU, indicating an interaction of the barbiturate anion with EtAd or the adeninium cation.

The reference experiment of EtAd with **4c** shows also a response of the chromophore, indicating a salt formation and no supramolecular complex formation as primary reaction (Supporting Information, Figure S9). A K_A of $300 \pm 40\ L\,mol^{-1}$ was found, which is smaller than that for **4b** with EtAd (Supporting Information, Table S8).

A titration of the anionic form of **4b**, which is generated by DBU addition, with EtAd did not show any shift of the UV/Vis absorption maximum. This is an indication that the adeninium cation forms a moderately strong complex with **3b**.

This complex formation influences the equilibrium of the acid–base reaction, resulting in a higher association constant by a reaction of **4b** instead of **4c**. This could be an explanation for the hypsochromic shift compared to salt formation with DBU or BuCy.

A ^1H NMR titration of **4b** with EtAd was not possible, owing to insolubility of the generated salt in CD_2Cl_2. The resulting solid was isolated and investigated by NMR spectroscopy in [D_6]DMSO. The reference experiment of EtAd with 1,1,1-trifluoroacetic acid in [D_6]DMSO is given in the Supporting Information (Figure S15), which shows the corresponding result for an acid–base interaction.

Solid-state structure of 4b/EtAd

Deep-red crystals were obtained by crystallisation of a 1:1 mixture of **4b** with EtAd from MeOH/EtOAc suitable for single crystal X-ray diffraction studies. Compound **4b**/EtAd crystallises in the triclinic space group $P\bar{1}$. The structure of the asymmetric unit is shown in the Supporting Information (Figure S32) together with selected bond lengths and angles.

The solid state structure analysis confirms the salt formation (Figure S32). However, in contrast to **4b**/BuCy, the EtAd molecule in the solid structure of **4b**/EtAd is mono-protonated. **4b**/EtAd forms a 3D network by hydrogen bonds and π–π interactions. The barbiturate anions form dimers by two hydrogen bonds (III, Figure 10), which are additionally linked together by two hydrogen bonds to the adeninium cation (I and II, Figure 10). This structure is stabilised by π–π interactions (Supporting Information, Figure S33, Scheme S7). Furthermore, the adeninium cation forms dimers by two hydrogen bonds (Fig-

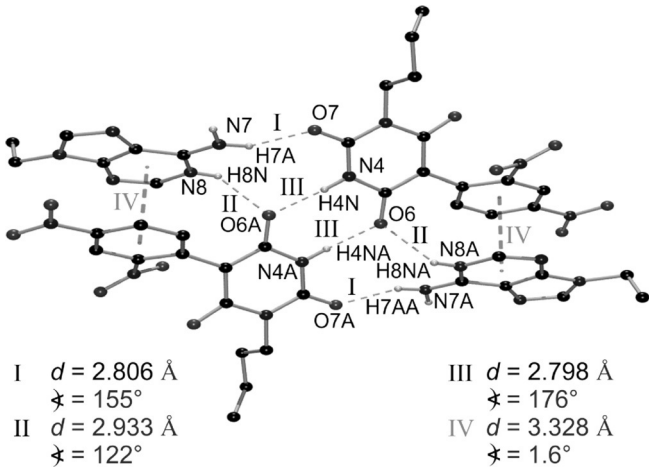

Figure 10. Selected detail of the crystal structure **4b**/EtAd. Grey dotted lines indicate intermolecular hydrogen bonds of type I–III, with *d* giving the D···A distance and ∢ the D–H···A angle. Thicker dotted lines indicate intermolecular π–π interactions between aromatic rings, with *d* giving in the centroid to centroid distance and ∢ the interplanar angle of interacting rings. All C-bonded hydrogen atoms are omitted for clarity.

ure S33), which link those structures together to result in a 3D network.[24]

9-Ethylguanine

Titration experiments with 9-ethylguanine (EtGu) as receptor were difficult to perform because of the poor solubility of this nucleobase derivative, especially in CH_2Cl_2 and in CH_2Cl_2/MeOH. Therefore, complex titration could only be carried out in a small concentration range of EtGu (Supporting Information, Figure S10). The UV/Vis spectroscopic complex titration of **4b** with EtGu in a mixture of CH_2Cl_2/MeOH (ratio 25:1, v/v) results in an association constant of $K_A = 500 \pm 80\ L\,mol^{-1}$ (Supporting Information, Table S9). This value for the genuine salt formation is in good accordance with the lower basicity of EtGu ($pK_a = 3.30$).[22] The UV/Vis absorption spectra of **4b** with EtGu are similar to those of **4b** with BuCy. A preferred complexation of the enol species with the BA derivative leads to a bathochromic shift of the former UV/Vis absorption at 377 nm. At higher concentrations, a second UV/Vis absorption maximum at 438 nm appears which indicates the formation of the enolate species. No statements could be made on the concurrence of complexation versus genuine salt formation, because of the too low concentration range. Owing to the insolubility of EtGu in CH_2Cl_2, NMR titration experiments could not be carried out.

1-n-Butylthymine

The nucleobase 1-*n*-butylthymine BuTy shows the same hydrogen bonding sequence as BA in the keto form. Therefore, a complexation is possible when two hydrogen bonds are involved. Indeed, this type of complex formation should not influence the keto–enol tautomerism. Furthermore, thymine is that nucleobase which is not strong basic ($pK_a = 9.9$)[22] and therefore genuine salt formation is not expected. Thus, the UV/Vis titration of **4b** with BuTy (Supporting Information, Figure S12, Table S11) shows no significant changes in the spectrum above 300 nm. Thus, BuTy has no measurable influence on tautomerism of **4b**.

2,6-Diacetamidopyridine

2,6-Diaminopyridine derivatives as 2,6-diacetamidopyridine (DACP) are often used as supramolecular complexation agents for BA because of the hydrogen bonding sequence (DAD), which is complementary to that of the keto form (ADA) of **4b**.[7a,11] As described above, this complexation should not influence the keto–enol tautomerism of **4b**. A pK_a value of DACP could not be found. Data of related compounds such as pyridine ($pK_a = 5.17$) and 2-acetamidopyridine ($pK_a = 4.09$)[22] indicate that the pK_a of DACP is likely to be about 3, which is analogous to basicity of EtGu, and thus salt formation is expected.

The measured plot of the UV/Vis absorbance of **4b** at 443 nm as function of the DACP concentration could not be evaluated with Equation (6) (Supporting Information, Figure S11, Table S10). Surprisingly, the reference experiment DACP with **4c** shows no UV/Vis spectroscopic respond in spite of its comparable acidity (Table 1). This result suggests that salt formation of weak basic receptors only occurs if a suitable hydrogen bonding pattern is available.

This phenomenon is called cooperativity and is usually evaluated by plotting *r*/*x* as a function of *r*, the so called Scatchard plot,[25] where *r* is ΔA [Eq. (6)] and $x = [DACP]$. The shapes of the Scatchard plots are concave downward curves for positive cooperativity, straight lines for no cooperativity, and concave upward curves for negative cooperativity.[26] The obtained curve for the titration of **4b** with DACP shows the typical behaviour for a negative cooperativity (Figure 11).[27]

Cooperativity as well as the suggested 1:2 stoichiometry of the complex formation are results of the hydrogen bonding sequences of **4b** (ADA) and DACP (DAD). After the proton trans-

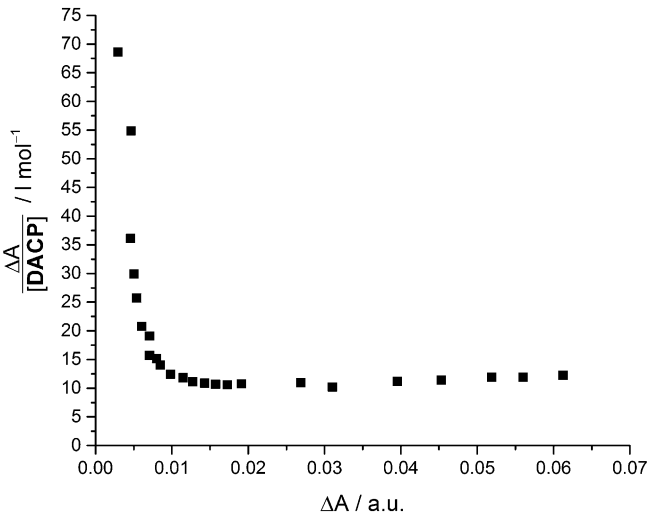

Figure 11. Scatchard plot of the UV/Vis titration of **4b** with DACP in CH_2Cl_2.

fer, the sequence of the BA remains ADA, but $DACP^+$ changes to a DDD sequence. This makes the protonated $DACP^+$ unsuitable for a complexation of **4b** or the BA anion, while the neutral DACP is suited for complex formation with **4b** and the BA anion. Thus, one DACP is protonated and a second molecule was necessary for complex formation with the BA anion, resulting in the 1:2 stoichiometry (Supporting Information, Scheme S1). Such cooperative systems are described for example with oligo-bipyridines as metal ligands.[26]

Structure of 4b/DACP in the solid state

Deep-red crystals suitable for single crystal X-ray diffraction studies were obtained by crystallisation of a 1:1 mixture of **4b** with DACP from CH_2Cl_2/*n*-pentane. Compound **4b**/DACP crystallises in the triclinic space group $P2_1/c$ (Supporting Information, Figure S36).

The sp^2 C8 atom and the given bond lengths as observed and discussed for **4b**/BuCy, verify the formation of a barbiturate anion as the sum of its bond angles is 359.7(7) (Supporting Information, Figure S36).

In the solid state, **4b**/DACP develops a 3D network, formed by 2D layers, which are linked together by π–π interactions. The 2D layers are formed by dimers of barbiturate anions, which are held together by two hydrogen bonds (IV; Figure 12). Furthermore, DACP is stabilising a proton with two intramolecular hydrogen bonds (I and II; Figure 12). Thereby, the NH-hydrogen bond donor functionalities were rotated outwards and are able to link the barbiturate anions together in crystallographic *b* and *c* axis. These hydrogen bonds were supported by π–π interactions within this layer (Figure 12). An additional π–π interaction link the layers in crystallographic *a* axis together to form a 3D network (Supporting Information, Figure S37, Scheme S9).

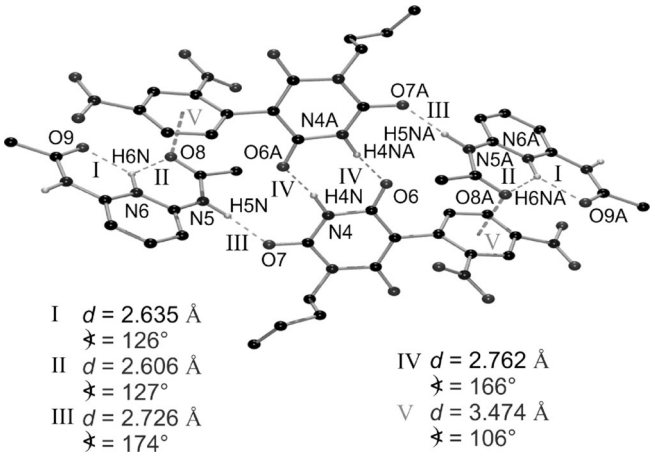

Figure 12. Detail of the crystal structure of **4b**/DACP. Grey dotted lines indicate intermolecular hydrogen bonds of type I–IV, with *d* giving the D···A distance and ∢ the D–H···A angle. Thicker dotted lines indicate intermolecular π–π interactions between aromatic rings, with *d* giving in the centroid to centroid distance and ∢ the interplanar angle of interacting rings. All C-bonded hydrogen atoms are omitted for clarity.

Conclusion

The pK_a vales of the BAs are in the range of 0.0 for the 5-(2,4-dinitrophenyl)-barbituric acid derivatives **4a–c** and 1.3 for 5-{4-[(1,3-dioxo-1*H*-inden-2(3*H*)-ylidene)methyl]phenyl} barbituric derivatives **7b,c**. Therefore, when a huge excess even of a weak base, such as a common solvent, is used, readily the anionic form is developed in great extent. This feature determines significantly the UV/Vis spectroscopic properties of the BA derivatives **4a–c** and **7b,c**.

The evaluation of the UV/Vis absorption maxima ($\tilde{\nu}_{max}$) as function of solvent property shows that the present anionic form of the BA derivatives is mostly affected by the solvents HBD properties. $\tilde{\nu}_{max}$ shifts hypsochromically with increasing HBD strength or acidity of solvent. HBA or basicity of solvent properties causes additionally a positive solvatochromic effect on $\tilde{\nu}_{max}$ as long as NH moieties of the BA derivative are not barricaded. Increase of dipolarity/polarizability of solvents cause also a bathochromic shift of $\tilde{\nu}_{max}$ as shown by the regression coefficients determined from the LFE relationships of Kamlet–Taft and Catalán.

The mono *N*-(*n*-butyl)-substituted barbituric acids **4b** and **7b** have been found suitable to examine the interaction with nucleobase derivatives and structurally related receptors. The results have shown that each of the used receptors 1-*n*-butylthymine, 9-ethyladenine, 1-*n*-butylcytosine, 9-ethylguanine, and 2,6-diacetamidopyridine, respectively, interacts in another way with **4b** or **7b**. Of course, acid–base reactions take place as expected, which is deduced from the pK_a. The formed ionic species can interact in many ways with each other by supramolecular complex formation as shown in Figure 13 and summarised in the Supporting Information, Table S12.

Advantageously, the potentiality of the BA species to interact with HB donor or acceptor molecules can be precisely measured by employing the coefficients derived from the Kamlet–Taft or Catalán LFE relationships. The results of supramolecular complex formation and solvatochromism study match amazingly to the point that negatively charged BA moieties still can show a HBD property. As consequence of this result, the anticipation of the reality of those BA/receptor pairs is very difficult to project in a synthetic concept for a suitable probe dye. The reason for this conclusion is that many interactions can simultaneously play a role as shown in the summarising Figure 13.

Too strong acidic compounds are unsuitable because genuine salt formation dominates. Weaker acids do interact in a smaller extend (lower K_A), but supramolecular complex formation dominates over genuine salt formation. Therefore, the focus of further studies must lie on weaker acidic dyes ($pK_a > 2.0$), which show a strong optical response.

The precise adjusting of the optimised pK_a of BA dyes for supramolecular complex formation is objective of further studies.

Experimental Section

The receptors 1-butylcytosine BuCy,[28] 1-butylthymine BuTy,[29] 9-ethyladenine EtAd,[30] and 2,6-diacetamidopyridine DACP[31] were

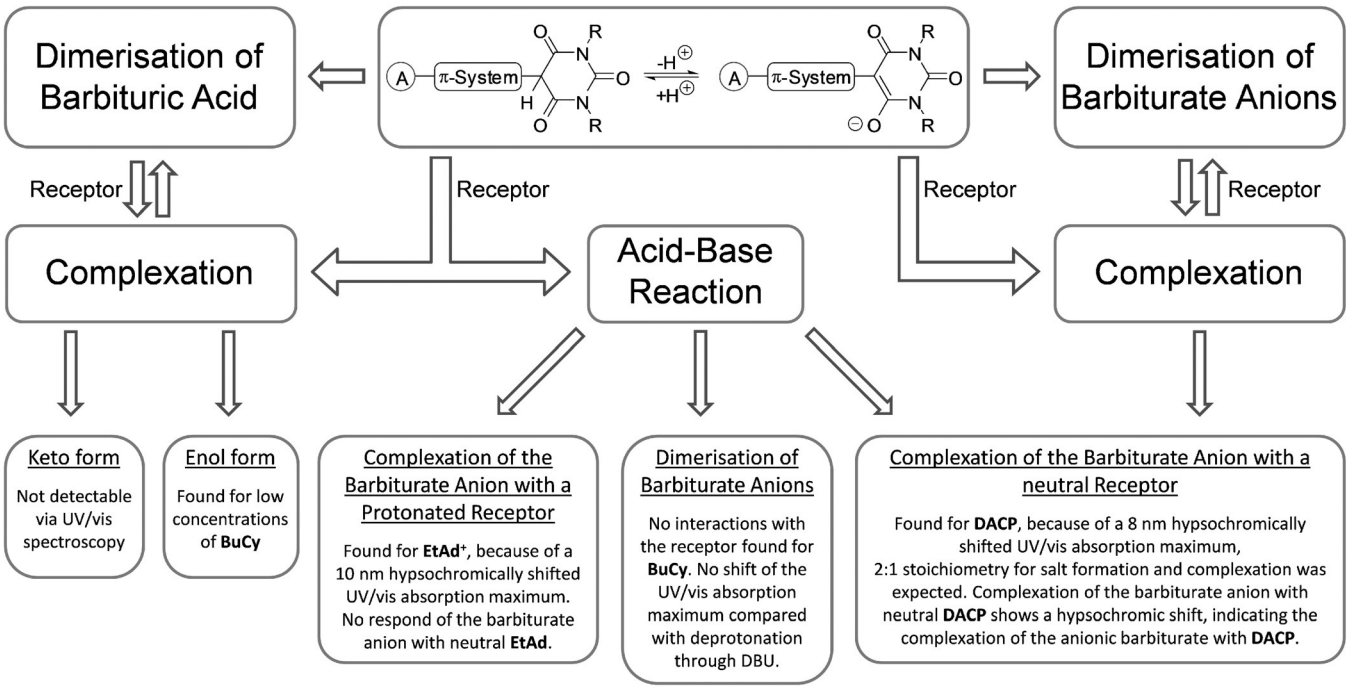

Figure 13. Overview on possible interactions of enolizable barbiturate dyes with different receptors. A = acceptor functionality.

synthesised according to previous reports. 9-Ethylguanine EtGu was received from Sigma Aldrich (≥98%) and was used as received.

The solvents dichloromethane and methanol were dried and freshly distilled before use. *N*,*N*-Dimethyl formamide (99.8% spectroscopic grade, extra dry, Acros) was used without further purification. The UV/Vis spectroscopic measurements were carried out with a MCS 400 diode array spectrometer by Carl Zeiss Jena GmbH. The given melting temperatures indicate the beginning of melting. All solutions were freshly prepared immediately before the titrations.

5-(2,4-Dinitrophenyl)barbituric acid (4a): A solution of barbituric acid (0.600 g, 4.684 mmol) in anhydrous DMF (30 mL) was treated with sodium hydride (0.112 g, 4.684 mmol) to form the barbituric acid sodium salt. Then, the barbiturate solution was given into a solution of 2,4-dinitrofluorobenzene (1.000 g, 5.37 mmol) in DMF (10 mL). The solution was stirred for 1 h at ambient temperature and quenched with an excess of aqueous $Ca(OH)_2$. The solid by-product was filtered off and the DMF solution was dropped into ice/H_2SO_4. The precipitating solid was filtered off, washed with water and dried. For purification, the raw product is re-dissolved in an aqueous $NaHCO_3$ solution and impurities were extracted with CH_2Cl_2. After acidification of the aqueous phase with HCl, water was evaporated until a solid precipitate formed. The solid was filtered off, dried under reduced pressure, and recrystallised from ethanol.

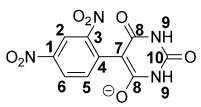

Overall yield 24%, yellow solid, mp: 165 °C; ^{1}H NMR ([D$_6$]DMSO-enol/enolate): δ = 7.98 (d, $^3J_{HH}$ = 9 Hz, 1H, ^{5}CH), 8.33 (d, $^3J_{HH}$ = 8 Hz, 1H, ^{6}CH), 8.52 (s, 1H, ^{2}CH), 10.46 ppm (s, 2H, ^{9}NH); ^{13}C NMR ([D$_6$]DMSO): δ = 88.4 (^{7}C), 120.1 (^{2}CH), 126.0 (^{6}CH), 134.8 (^{5}CH), 137.5, 143.8, 148.4 (^{1}C, ^{3}C, ^{4}C), 151.0 ($^{1\circ}$C), 162.7 ppm (^{8}C); elemental analysis (%) for $C_{10}H_6N_4O_7$ (294.18 g mol^{-1}): calcd: C 40.83, H 2.06, N 19.05; found: C 39.39, H 2.68, N 18.12; IR: $\tilde{\nu}$ = 3520, 3416, 3100, 2970, 2805, 1703, 1601, 1512, 1458, 1420, 1342, 1061, 996, 878, 837, 778, 760, 745, 722, 673, 579, 531 cm^{-1}.

1-*n*-Butyl-5-(2,4-dinitrophenyl)barbituric acid (4b): A solution of 1-*n*-butyl barbituric acid (0.863 g, 4.484 mmol) in anhydrous DMF (20 mL) was treated with 0.120 g (5.02 mmol) of sodium hydride to form the barbituric acid sodium salt. Then, the barbiturate solution was given into a solution of 2,4-dinitrofluorobenzene (1.000 g, 5.37 mmol) in DMF (10 mL). The solution was stirred for 1 h at ambient temperature and quenched with an excess of aqueous $Ca(OH)_2$. The solid by-product was filtered off and the DMF solution was dropped into ice/H_2SO_4. The precipitating solid was filtered off, washed with water, and dried. For purification, the raw product was re-dissolved in an aqueous $NaHCO_3$ solution and impurities were extracted with CH_2Cl_2. After acidification of the aqueous phase with HCl, the water slurry was extracted with CH_2Cl_2. The organic phase was dried over $MgSO_4$, the solvent was evaporated, and the solid residue was dried under reduced pressure.

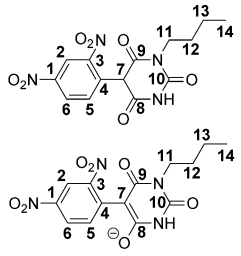

Overall yield 5%, yellow solid, mp: 79 °C; ^{1}H NMR ([D$_6$]DMSO-enol/enolate): δ = 0.87 (t, $^3J_{HH}$ = 7 Hz, 3H, ^{14}CH$_3$), 1.25 (m, 2H, ^{13}CH$_2$), 1.44 (m, 2H, ^{12}CH$_2$), 3.68 (t, $^3J_{HH}$ = 8 Hz, 2H, ^{11}CH$_2$), 8.07 (d, $^3J_{HH}$ = 8 Hz, 1H, ^{5}CH), 8.27 (d, $^3J_{HH}$ = 9 Hz, 1H, ^{6}CH), 8.47 (s, 1H, ^{2}CH), 10.37 ppm (s, 1H, ^{15}NH); ^{1}H NMR (CD_2Cl_2-keto): δ = 0.97 (t, $^3J_{HH}$ = 7 Hz, 3H, ^{14}CH$_3$), 1.39 (m, 2H, ^{13}CH$_2$), 1.61 (m, 2H, ^{12}CH$_2$), 3.91 (m, 2H, ^{11}CH$_2$), 5.02 (s, 1H, ^{7}CH), 7.79 (d, $^3J_{HH}$ = 9 Hz, 1H, ^{5}CH), 8.14 (s, 1H, ^{15}NH), 8.64 (dd, $^3J_{HH}$ = 9 Hz, $^3J_{HH}$ = 3 Hz, 1H, ^{6}CH), 9,14 ppm (d, $^3J_{HH}$ = 3 Hz, 1H, ^{2}CH), ^{13}C NMR ([D$_6$]DMSO): δ = 13.8 (^{14}CH$_3$), 19.6 (^{13}CH$_2$), 30.0 (^{12}CH$_2$), 38.6 (^{11}CH$_2$), 87.5 (^{7}C), 119.5 (^{2}CH), 125.1 (^{6}CH), 134.0 (^{5}CH), 142.6, 147.5, 150.7 (^{1}CH, ^{3}CH, ^{4}CH), 150.7 ($^{1\circ}$C), 160.2 (^{8}C), 162.1 ppm (^{9}C); elemental analysis (%) for $C_{14}H_{14}N_4O_7$ (329.19 g mol^{-1}): calcd: C 48.01, H 4.03, N 16.00; found: C 46.30,

H 4.10, N 15.28; IR: $\tilde{\nu}$ = 3212, 3108, 2963, 2934, 2873, 1713, 1678, 1607, 1530, 1439, 1412, 1379, 1343, 1296, 1229, 1200, 1150, 1098, 911, 835, 739, 716, 567, 517 cm^{-1}.

1,3-Dimethyl-5-(2,4-dinitrophenyl)barbituric acid (4c): A solution of 1,3-dimethyl barbituric acid (0.731 g, 4.684 mmol) in anhydrous DMF (30 mL) was treated with sodium hydride (0.112 g, 4.68 mmol) to form the barbituric acid sodium salt. Then, the barbiturate solution was given into a solution of 2,4-dinitrofluorobenzene (1.000 g, 5.37 mmol) in DMF (10 mL). The solution was stirred for 1 h at ambient temperature and quenched with an excess of aqueous $Ca(OH)_2$. The solid by-product was filtered off and the DMF solution was dropped into ice/H_2SO_4. The precipitating solid was filtered off, washed with water, and dried. For purification, the raw product is re-dissolved in an aqueous $NaHCO_3$ solution and impurities were extracted with CH_2Cl_2. After acidification of the aqueous phase with HCl, a solid precipitated, which was filtered off, washed with water, and dried under reduced pressure.

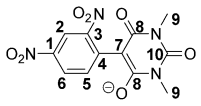

Overall yield 44%, yellow solid, mp: 195 °C; ^{1}H NMR ([D$_6$]DMSO-enol/enolate): δ = 3.14 (s, 6H, ^{9}CH$_3$), 8.10 (d, $^3J_{HH}$ = 5 Hz, 1H, ^{5}CH), 8.23 (ps, 1H, ^{6}CH), 8.45 ppm (s, 1H, ^{2}CH); ^{13}C NMR ([D$_6$]DMSO): δ = 27.5 (^{9}CH$_3$), 87.3 (^{7}C), 119.5 (^{2}CH), 124.7 (^{6}CH), 134.0 (^{5}CH), 140.1, 141.9, 147.2 (^{1}C, ^{3}C, ^{4}C), 151.9 ($^{1\circ}$C), 160.9 ppm (^{8}C); elemental analysis (%) for $C_{12}H_{10}N_4O_7$ (329.19 g mol^{-1}): calcd: C 44.73, H 3.13, N 17.39; found: C 44.64, H 3.18, N 17.26; IR: $\tilde{\nu}$ = 3110, 3081, 3052, 2865, 1696, 1677, 1605, 1530, 1441, 1426, 1379, 1343, 1312, 1283, 1246, 1152, 1115, 1082, 994, 924, 860, 828, 754, 725, 660, 629, 592, 538 cm^{-1}.

2-(4-Fluorobenzylidene)-1*H*-indene-1,3(2*H*)-dione (5): 1,3-indandione (2.90 g, 19.82 mmol) was heated in ethanol (100 mL) until the solid dissolved. 4-fluorobenzaldehyde (2.46 g, 19.82 mmol) and catalytic amounts of piperidine were added. The solution was stirred for 3 h under reflux, cooled to ambient temperature, and the crystallised solid was filtered of, washed with ethanol, and recrystallised from ethanol.

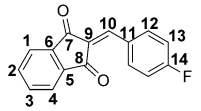

Yield 81%, yellow solid, mp: 178 °C; ^{1}H NMR ([D$_6$]DMSO): δ = 7.41 (dd, $^3J_{HH}$ = 9 Hz, $^3J_{HF}$ = 9 Hz, 2H, ^{13}CH),7.86 (s, 1H, $^{1\circ}$CH), 7.96 (m, 4H, $^{1-4}$CH), 8.62 ppm (dd, $^3J_{HH}$ = 9 Hz, $^4J_{HF}$ = 6 Hz, 2H, ^{12}CH); ^{13}C NMR ([D$_6$]DMSO): δ = 116.0 (d, $^2J_{CF}$ = 22 Hz, ^{13}CH), 123.1, 123,2 (^{2}CH, ^{3}CH), 128.9 (d, $^6J_{CF}$ = 3 Hz, ^{9}C), 129.6 (d, $^4J_{CF}$ = 4 Hz, ^{11}C), 136.0, 136.1 (^{1}CH, ^{4}CH), 136.9 (d, $^3J_{CF}$ = 9 Hz, ^{12}CH), 139.5, 141.9 (^{5}C, ^{6}C), 144.2 ($^{1\circ}$CH), 164.8 (d, $^1J_{CF}$ = 254 Hz, ^{14}C), 188.8, 189.4 ppm (^{7}C, ^{8}C); elemental analysis (%) for $C_{16}H_9FO_2$ (252.24 g mol^{-1}): calcd: C 76.19, H 3.60; found: C 76.18, H 3.62; IR: $\tilde{\nu}$ = 3096, 3073, 3040, 1730, 1690, 1580, 1506, 1420, 1371, 1227, 1200, 1165, 1072, 992, 835, 733, 513, 497, 411 cm^{-1}.

1-*n*-Butyl-5-(4-((1,3-dioxo-1*H*-inden-2(3*H*)-ylidene) methyl)phenyl)barbituric acid (7b): The potassium salt of 1-*n*-butyl-barbituric acid (444 mg, 2.00 mmol) was dissolved in anhydrous DMF (50 mL). $CaCO_3$ (300 mg, 3.00 mmol) and **5** (252 mg, 1.00 mmol) were added in a single portion and the reaction mixture was heated at 150 °C for 8 h. The intense violet-coloured solution was cooled down to ambient temperature, filtered, and poured onto ice/H_2SO_4. The precipitating solid was filtered off, dissolved in CH_2Cl_2 and washed twice with 100 mL of a $NaHCO_3$ solution. The red-coloured aqueous solution was extracted twice with CH_2Cl_2 (100 mL) to remove impurities. After acidification with HCl, the aqueous phase was extracted twice with CH_2Cl_2 (100 mL). The organic phase was dried over $MgSO_4$, evaporated, and the obtained solid was dried under reduced pressure.

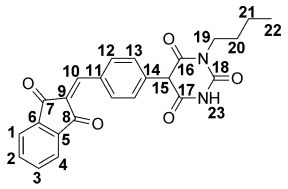

Yield 8%, orange solid, mp:122 °C; ^{1}H NMR (CD_2Cl_2-keto): δ = 0.94 (t, $^3J_{HH}$ = 7 Hz, 3H, ^{22}CH$_3$), 1.34 (m, 2H, ^{21}CH$_2$), 1.57 (m, 2H, $^{2\circ}$CH$_2$), 3.89 (t, $^3J_{HH}$ = 7 Hz, 2H, ^{19}CH$_2$), 4.75 (s, 1H, ^{15}CH), 7.42 (d, $^3J_{HH}$ = 8 Hz, 2H, ^{13}CH), 7.86 (d, $^3J_{HH}$ = 9 Hz, 2H, ^{1}CH, ^{4}CH), 7.86 (s, 1H, $^{1\circ}$CH), 8.01 (m, 2H, ^{2}CH, ^{3}CH), 8.48 ppm (d, $^3J_{HH}$ = 8 Hz, 2H, ^{12}CH); IR: $\tilde{\nu}$ = 2960, 2923, 2857, 1677, 1588, 1509, 1443, 1416, 1370, 1354, 1254, 1190, 1076, 1018, 990, 795, 764, 733, 670, 538, 505, 422 cm^{-1}.

1,3-Dimethyl-5-(4-((1,3-dioxo-1*H*-inden-2(3*H*)-ylidene) methyl)-phenyl)barbituric acid (7c): The potassium salt of 1,3-dimethyl-barbituric acid (300 mg, 1.65 mmol) was dissolved in anhydrous DMF (20 mL). $CaCO_3$ (275 mg, 2.75 mmol) and **5** (215 mg, 0.852 mmol) were added in a single portion and the reaction mixture was heated at 150 °C for 4 h. The intense violet-coloured solution was cooled down to ambient temperature, filtered and poured onto ice/H_2SO_4. The precipitating solid was filtered off, dissolved in CH_2Cl_2, and washed twice with a $NaHCO_3$ solution (100 mL). The red-coloured aqueous solution was extracted twice with CH_2Cl_2 (100 mL) to remove impurities. After acidification with HCl, the aqueous phase was extracted twice with CH_2Cl_2. This organic phase was dried over $MgSO_4$, evaporated, and the obtained solid was dried under reduced pressure.

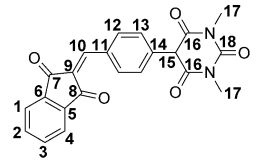

Yield 75%, orange solid, mp: 220 °C; ^{1}H NMR (CD_2Cl_2): δ = 3.35 (s, 6H, ^{17}CH$_3$), 4.78 (s, 1H, ^{15}CH), 7.40 (d, $^3J_{HH}$ = 8 Hz, 2H, ^{13}CH), 7.85 (d, $^3J_{HH}$ = 9 Hz, 2H, ^{1}CH, ^{4}CH), 7.85 (s, 1H, $^{1\circ}$CH), 8.01 (m, 2H, ^{2}CH, ^{3}CH), 8.46 ppm (d, $^3J_{HH}$ = 8 Hz, 2H, ^{12}CH); ^{13}C NMR (CD_2Cl_2): δ = 29.2 (^{17}CH$_3$), 55.9 (^{15}CH), 123.6, 123.7 (^{1}CH, ^{4}CH), 129.2 (^{13}CH), 134.8 (^{12}CH), 135.8, 136.0 (^{3}CH, ^{4}CH), 130.5, 133.7, 138.5, 140.5, 142.9 (^{5}C, ^{6}C, ^{9}C, ^{11}C, ^{14}C), 145.2 ($^{1\circ}$CH), 151.7 (^{18}CO), 166.9 (^{16}CO), 189.2, 190.0 ppm (^{7}CO, ^{8}CO); elemental analysis (%) for $C_{22}H_{16}N_2O_5$ (388.37 g mol^{-1}): calcd: C 68.04, H 4.15, N 7.21; found: C 68.26, H 4.24, N 6.27; IR: $\tilde{\nu}$ = 1702, 1680, 1615, 1601, 1588, 1509, 1453, 1420, 1374, 1352, 1318, 1289, 1250, 1190, 1075, 990, 843, 795, 768, 735, 669, 588, 538, 505, 422 cm^{-1}.

X-ray crystallography

All data were collected with an Oxford Gemini S diffractometer. For data collection, cell refinement and data reduction the software CrysAlisPro was used.[32] All structures were solved by direct methods using SHELXS-2013 and refined by full-matrix least-squares procedures on F^2 using SHELXL-2013.[33] All non-hydrogen atoms were refined anisotropically. All C-bonded hydrogen atoms were refined using a riding model. The positions of N- and/or O-bonded hydrogen atoms were taken from difference Fourier maps and refined isotropically.

In case of **4b**/DACP, the atoms C11–C14 and the atoms N1, O1, and O2 were refined disordered with split occupancies of 0.25/0.75 and 0.59/0.41, respectively.

CCDC 1420547 (**4a**), 1420551 (**4c**), 1420548 (**4b**/BuCy), 1420550 (**4b**/EtAd), and 1420549 (**4b**/DACP) contain the supplementary crystallographic data for this paper. These data are provided free of charge by The Cambridge Crystallographic Data Centre. Tables of bond lengths, angles, and torsion angles are also given in the Supporting Information.

Acknowledgements

Financial support from the Fonds der Chemischen Industrieand the DFG (Deutsche Forschungsgemeinschaft)SP 392/26-1/26-3is gratefully acknowledged.

Keywords: barbituric acid · keto–enol tautomerism · molecular recognition · nucleobases · solvatochromism · UV/Vis spectroscopy

[1] J. D. Watson, F. Crick, *Nature* **1953**, *171*, 737 – 738.
[2] a) J. Sartorius, H.-J. Schneider, *Chem. Eur. J.* **1996**, *2*, 1446 – 1452; b) A. M. Kelly-Rowley, V. M. Lynch, E. V. Anslyn, *J. Am. Chem. Soc.* **1995**, *117*, 3438 – 3447; c) U. Lüning, C. Kühl, A. Uphoff, *Eur. J. Org. Chem.* **2002**, 4063 – 4070.
[3] Y. Kyogoku, R. C. Lord, A. Rich, *Nature* **1968**, *218*, 69 – 72.
[4] G. A. Jeffrey, J. Mitra, *Acta Crystallogr.* **1983**, *B39*, 469 – 480.
[5] a) C. Vilaivan, W. Srinarang, N. Yotapan, W. Mansawat, C. Boonlua, J. Kawakami, Y. Yamaguchi, Y. Tanaka, T. Vilaivan, *Org. Biomol. Chem.* **2013**, *11*, 2310 – 2317; b) A. B. Eldrup, C. Christensen, G. Haaima, P. E. Nielsen, *J. Am. Chem. Soc.* **2002**, *124*, 3254 – 3262; c) A. B. Eldrup, B. B. Nielsen, G. Haaima, H. Rasmussen, J. S. Kastrup, C. Christensen, P. E. Nielsen, *Eur. J. Org. Chem.* **2001**, 1781 – 1790.
[6] A. C. Cheng, W. W. Chen, C. N. Fuhrmann, A. D. Frankel, *J. Mol. Biol.* **2003**, *327*, 781 – 796.
[7] a) I. Bolz, S. Spange, *Chem. Eur. J.* **2008**, *14*, 9338 – 9346; b) I. Bolz, D. Schaarschmidt, T. Rüffer, H. Lang, S. Spange, *Angew. Chem.* **2009**, *121*, 7576 – 7579; c) M. Bauer, S. Spange, *Eur. J. Org. Chem.* **2010**, 259 – 264.
[8] a) Y. Kyogoku, R. C. Lord, A. Rich, *J. Am. Chem. Soc.* **1967**, *89*, 496 – 504; b) F. Würthner, S. Yao, T. Debaerdemaeker, R. Wortmann, *J. Am. Chem. Soc.* **2002**, *124*, 9431 – 9447; c) N. S. Nudelman, C. E. S. Alvaro, *J. Phys. Org. Chem.* **2011**, *24*, 1067 – 1071; d) C. Reichardt, T. Welton, *Solvents and Solvent Effects in Organic Chemistry*, Wiley-VCH, Weinheim, **2011**, p. 359 – 424.
[9] a) R. Puig-de-la-Bellacasa, L. Giménez, S. Pettersson, R. Pascual, E. Gonzalo, J. A. Esté, B. Clotet, J. I. Borrell, J. Teixidó, *Eur. J. Med. Chem.* **2012**, *54*, 159 – 174; b) I. Bolz, M. Bauer, A. Rollberg, S. Spange, *Macromol. Symp.* **2010**, *287*, 8 – 15.
[10] a) S. S. Joshi, I. R. Gambhir, *J. Am. Chem. Soc.* **1956**, *78*, 2222 – 2224; b) I. M. Fellows, D. E. Kaelin, S. F. Martin, *J. Am. Chem. Soc.* **2000**, *122*, 10781 – 10787.
[11] M. Bauer, S. Spange, *Angew. Chem.* **2011**, *123*, 9901 – 9904.
[12] V. N. Khrustalev, K. A. Krasnov, T. V. Timofeeva, *J. Mol. Struct.* **2008**, *878*, 40 – 49.
[13] a) T. Yokoyama, R. W. Taft, M. J. Kamlet, *J. Am. Chem. Soc.* **1976**, *98*, 3233 – 3237; b) R. W. Taft, M. J. Kamlet, *J. Am. Chem. Soc.* **1976**, *98*, 2886 – 2894; c) M. J. Kamlet, J.-L. M. Abboud, R. W. Taft, *J. Am. Chem. Soc.* **1977**, *99*, 6027 – 6038; d) M. J. Kamlet, T. N. Hall, J. Boykin, R. W. Taft, *J. Org. Chem.* **1979**, *44*, 2599 – 2604; e) R. W. Taft, M. J. Kamlet, *J. Chem. Soc. Perkin Trans. 2* **1979**, 1723 – 1727; f) M. J. Kamlet, R. W. Taft, *J. Chem. Soc. Perkin Trans. 2* **1979**, 349 – 356; g) M. J. Kamlet, J.-L. M. Abboud, M. H. Abraham, R. W. Taft, *J. Org. Chem.* **1983**, *48*, 2877 – 2887.
[14] a) J. Catalán, V. López, P. Pérez, *Liebigs Ann.* **1995**, 793 – 795; b) J. Catalán, V. López, P. Pérez, R. Martín-Villamil, J.-G. Rodríguez, *Liebigs Ann.* **1995**, 241 – 252; c) J. Catalán, C. Díaz, V. López, P. Pérez, J.-L. G. d. Paz, J. G. Rodríguez, *Liebigs Ann.* **1996**, 1785 – 1794; d) J. Catalán, C. Díaz, *Liebigs Ann.* **1997**, 1941 – 1949; e) J. Catalán, J. Palomar, C. Díaz, J.-L. G. d. Paz, *J. Phys. Chem. A* **1997**, *101*, 5183 – 5189; f) J. Catalán, C. Díaz, *Eur. J. Org. Chem.* **1999**, 885 – 891; g) J. Catalán, H. Hopf, *Eur. J. Org. Chem.* **2004**, 4694 – 4702; h) J. Catalán, *J. Phys. Chem. B* **2009**, *113*, 5951 – 5960.
[15] a) A. Schade, R. Menzel, H. Görls, S. Spange, R. Beckert, *Asian J. Org. Chem.* **2013**, *2*, 498 – 503; b) K. Hofmann, S. Spange, *J. Org. Chem.* **2012**, *77*, 5049 – 5055; c) A. Oehlke, A. A. Auer, I. Jahre, B. Walfort, T. Rüffer, P. Zoufalá, H. Lang, S. Spange, *J. Org. Chem.* **2007**, *72*, 4328 – 4339; d) M. Bauer, A. Rollberg, A. Barth, S. Spange, *Eur. J. Org. Chem.* **2008**, 4475 – 4481; e) K. Schreiter, S. Spange, *J. Phys. Org. Chem.* **2008**, *21*, 242 – 250; f) K. Hofmann, K. Schreiter, A. Seifert, T. Rüffer, H. Lang, S. Spange, *New J. Chem.* **2008**, *32*, 2180 – 2188; g) F. Riedel, S. Spange, *J. Phys. Org. Chem.* **2012**, *25*, 1261 – 1268; h) S. Seifert, A. Seifert, G. Brunklaus, K. Hofmann, T. Ruffer, H. Lang, S. Spange, *New J. Chem.* **2012**, *36*, 674 – 684.
[16] a) S. F. Oğuz, I. Doğan, *Spectrosc. Lett.* **2004**, *37*, 607 – 618; b) P. De Meester, S. S. C. Chu, M. V. Jovanovic, E. R. Biehl, *J. Heterocycl. Chem.* **1986**, *23*, 337 – 341; c) F. Zuccarello, G. Buemi, C. Gandolfo, A. Contino, *Spectrochim. Acta Part A* **2003**, *59*, 139 – 151.
[17] K. A. Connors, *Binding Constats*, New York, Chichester, Brisbane, Toronto, Singapore, **1987**, p. 169 – 171.
[18] H. Koffer, *J. Chem. Soc. Perkin Trans. 2* **1974**, 1428 – 1429.
[19] A. Schade, N. Behme, S. Spange, *Chem. Eur. J.* **2014**, *20*, 2232 – 2243.
[20] G. Wypych, *Handbook of Solvents*, ChemTee Publishing, Toronto, **2014**, p. 581 – 621.
[21] C. Reichardt, *Chem. Rev.* **1994**, *94*, 2319 – 2358.
[22] http://research.chem.psu.edu/brpgroup/pKa_compilation.pdf, *22.06.2015*.
[23] N. Bošnjaković-Pavlović, A. Spasojević-de Biré, *J. Phys. Chem. A* **2010**, *114*, 10664 – 10675.
[24] B. Sridhar, K. Ravikumar, *Acta Crystallogr.* **2007**, *C63*, o415 – o418.
[25] a) B. Perlmutter-Hayman, *Acc. Chem. Res.* **1986**, *19*, 90 – 96; b) A. A. Saboouri, A. A. Moosavi-Movahedi, *Biochem. Educ.* **1994**, *22*, 48 – 49.
[26] A. Pfeil, J.-M. Lehn, *J. Chem. Soc. Chem. Commun.* **1992**, 838 – 840.
[27] A. K. Bordbar, A. A. Saboury, A. A. Moosavi-Movahedi, *Biochem. Educ.* **1996**, *24*, 172 – 175.
[28] D. L. Helfer, R. S. Hosmane, N. J. Leonard, *J. Org. Chem.* **1981**, *46*, 4803 – 4804.
[29] A. D. Hamilton, D. v. Engen, *J. Am. Chem. Soc.* **1987**, *109*, 5035 – 5036.
[30] J. S. Nowick, J. S. Chen, G. Noronha, *J. Am. Chem. Soc.* **1993**, *115*, 7636 – 7644.
[31] K. Kurita, R. L. Williams, *J. Heterocycl. Chem.* **1975**, *12*, 789 – 791.
[32] G. Sheldrick, *Acta Crystallogr. Sect. A* **2008**, *64*, 112 – 122.
[33] CyrsAlisPro, version 1.171.33.64 (release 22.03.2010 CrysAlis171.NET), Agilent Technologies.

Received: November 11, 2015
Published online on March 4, 2016